Journal of Computational and Applied Mathematics 433 (2023) 115319

Contents lists available at ScienceDirect

Journal of Computational and Applied Mathematics

journal homepage: www.elsevier.com/locate/cam

Binary thermal fluids computation over arbitrary surfaces with second-order accuracy and unconditional energy stability based on phase-field model

Qing Xia [a], Yuehan Liu [a], Junseok Kim [b], Yibao Li [a,*]

[a] School of Mathematics and Statistics, Xi'an Jiaotong University, Xi'an 710049, China
[b] Department of Mathematics, Korea University, Seoul 02841, Republic of Korea

ARTICLE INFO

Article history:
Received 14 July 2022
Received in revised form 30 December 2022

Keywords:
Two-phase flow
Laplace–Beltrami operator
Heat convection
Unconditional energy stability
Second-order accuracy
Multiple physical field coupling

ABSTRACT

In this paper, we propose an efficient surface computational system with second-order spatial and temporal accuracy to solve multiple physical field coupling problems over arbitrary surfaces. The computational system is coupled with heat transfer equation and incompressible Navier–Stokes equation based on a phase-field model. Due to the discretization of the triangular grids, we define the discretized gradient operator, divergence operator and the Laplace–Beltrami operator with second-order spatial accuracy. The Crank–Nicolson-type scheme is used to confirm the temporal accuracy. The Navier–Stokes equation is solved by the projection method. We use the biconjugate gradient stabilized method to solve the involved equations. The discrete system is provable to be unconditionally stable and the mass conservation law is satisfied during the computation, which implies that the proposed method is not limited by the temporal step. Several computational tests are conducted to show the efficiency, robustness and accuracy of the proposed scheme.

1. Introduction

Surface computation over arbitrary manifolds is widely used in many essential and practical problems such as medical processing [1–3], variational design of curves [4,5], additive manufacturing [6,7]. The current research method for solving partial differential equations on arbitrary surfaces, which was first systematically investigated at 1988 [8], can be divided into two categories: embedded narrow-band methods [9,10] and direct methods [11,12]. The narrow-band methods extended the partial differential equation (PDE) on surface to a high-dimensional space. By choosing a narrow band around the surface, the differential operator could be modified and the solution was restricted to the surface [13]. This approach was able to apply the surface computation over curved surfaces while retaining the simplicity and efficiency in standard Cartesian coordinates. Bertalmío et al. [14] performed the embedding method to solve the variational problem and the resulting Euler–Lagrange evolution PDEs on surfaces. According to their approach, the underlying surface was represented as a level set of high-dimensional functions corresponding to the surface. This allowed the equations to be discretized and solved using a Cartesian grid method. A further improvement to this method was proposed by Greer [15]. The evolution

* Corresponding author.
E-mail address: yibaoli@xjtu.edu.cn (Y. Li).

https://doi.org/10.1016/j.cam.2023.115319
0377-0427/

equations were modified to maintain greater regularity of the solution near the surface, while the stability of the final solution cannot be well maintained. Fuselier et al. [16] proposed a higher-order kernel method for computationally solving the diffusion and reaction–diffusion PDEs on smooth closed surfaces embedded in R^d. This method required only the nodes and the corresponding normal vectors at discrete locations on the surface. However, the embedding methods had some limitations [17–19], since they do not allow for bounded open surfaces or objects of two or higher dimensions, which created complications in the finite numerical band around the surface. Such narrow bands required imposing the appropriate boundary conditions, however there were no general consensus on how to impose these conditions [20].

The direct methods define the discrete operators on the manifolds and use the information of the triangular mesh, i.e. the location of points, link relation of the triangle and the normal vector of the triangles, to solve the dynamical systems [21]. Chen and Wu [11,12] defined the Laplace–Beltrami operator over the regular surfaces with a discrete approximation. Xiao et al. [22] proposed a local tangential lifting method, which transformed the local surface problem to a local two dimensional problem with the selected surface nodes. Sun et al. [23] projected the surfactant model onto arbitrary surfaces based on the extensive investigation [24] in regular Euclidean Space. Suchde and Kuhnert [25] proposed a fully Lagrangian framework to capture the movement of the evolving surface, which was discretized with a cloud of numerical points. This method was borrowed from the lifting method. By applying the phase field method, which has obtained extensive attention on range of problems such as topology optimization with fluids [26] and solids [27], image processing [28], and copolymer mixtures [29], Li el al. [30] improved the accuracy of the lifting method and first proved the unconditional energy stability. Their method did not involve time step restrictions. Then, they extended the CH system to multi-component framework with second order unconditional accuracy [31]. Xia et al. [32] proposed a simple high-order method for computing the discrete gradient over arbitrary surfaces. Under the heuristic guidance of [33,34], the complicated system coupled with the incompressible Navier–Stokes equation and the phase-field model was first proved to be unconditionally stable with second-order accuracy.

In this paper, we propose a new surface computational method based on the phase field model to simulate the motion of heat flow over arbitrary surfaces. We construct a completely new system by coupling the heat conduction equation with the NS equation based on the phase-field model. The method constructs the corresponding discrete operators directly on the surface with guaranteed accuracy. We applied the Crank–Nicolson method to obtain the second-order accuracy. The discrete system is decoupled and converted to be a linear system, which can be solved by a biconjugate gradient stabilized method. The discrete system is proved to be unconditionally stable, which implies that we can use large time step. To our best knowledge, this is the first attempt for the simulation of thermal fluid motion over arbitrary surfaces. Various numerical experiments are simulated to verify the significance of the application of the model.

The remainder of this paper is organized as follows: We establish the binary thermal fluids model over arbitrary surfaces in Section 2. In Section 3, we provide the detailed illustrations of the proposed Crank–Nicolson-type scheme with temporally and spatially second-order accuracy. Then, we prove the unconditional energy stability of the system. Many computational tests are performed in Section 4. Finally, concluding remarks are given in Section 5.

2. Thermodynamic system based on phase-field model

We develop a system for the surface computation of simulating thermal flow motion on arbitrary surfaces inspired by the existing studies [32,35], which was consisted of the heat transfer equation coupled the incompressible NS equation based on the phase-field model over the arbitrary surfaces $S \subset \mathbb{R}^3$ as:

$$\frac{\partial \phi(\mathbf{x},t)}{\partial t} = \frac{1}{Pe}\Delta_S \mu(\mathbf{x},t) - \nabla_S \cdot (\phi(\mathbf{x},t)\mathbf{v}(\mathbf{x},t)), \tag{1a}$$

$$\mu(\mathbf{x},t) = f'(\phi(\mathbf{x},t)) - \epsilon^2 \Delta_S \phi(\mathbf{x},t), \tag{1b}$$

$$\rho\left(\frac{\partial \mathbf{v}(\mathbf{x},t)}{\partial t}\right) = -\nabla_S p(\mathbf{x},t) + \nabla_S \cdot \left(\eta \nabla_S \mathbf{v}(\mathbf{x},t)\right) - \frac{\sigma}{\epsilon}\phi(\mathbf{x},t)\nabla_S \mu(\mathbf{x},t) - \rho\left(\frac{\mathbf{v}(\mathbf{x},t)\cdot\nabla_S \mathbf{v}(\mathbf{x},t)}{2} + \frac{\nabla_S \cdot (\mathbf{v}(\mathbf{x},t)\otimes \mathbf{v}(\mathbf{x},t))}{2}\right), \tag{1c}$$

$$\nabla_S \cdot \mathbf{v}(\mathbf{x},t) = 0, \tag{1d}$$

$$\rho C_p\left(\frac{\partial T(\mathbf{x},t)}{\partial t}\right) = \nabla_S \cdot (k\nabla_S T(\mathbf{x},t)) - \rho C_p \mathbf{v}(\mathbf{x},t)\cdot\nabla_S T(\mathbf{x},t), \tag{1e}$$

where Δ_S and $\nabla_S\cdot$ denotes the tangential Laplace–Beltrami operator and the tangential divergence operator, respectively. Here, we use $f(\phi) = \phi^2(1-\phi)^2/4$ to define the double well bulk potential. The term $\mathbf{v}(\mathbf{x},t)\otimes\mathbf{v}(\mathbf{x},t)$ is used to denote the tensor product. The nonlinear advection term is treated as $\mathbf{v}\cdot\nabla_S\mathbf{v}/2+\nabla_S\cdot(\mathbf{v}\otimes\mathbf{v})/2$ with the divergence free condition, since $\mathbf{v}\cdot\nabla_S\mathbf{v} = \nabla_S\cdot(\mathbf{v}\otimes\mathbf{v})$ when $\nabla_S\cdot\mathbf{v} = 0$. This equivalent substitution is convenient for us to prove the unconditional energy stability and makes the discrete system avoid the stiffness influence caused by the convection. The intermediate variables $p(\mathbf{x},t)$ and $\mu(\mathbf{x},t)$ are the pressure and the chemical potential of the thermal fluid, respectively. The other dimensionless parameters are specified as following: the Peclet number Pe, the density ρ, the viscosity η, the surface tension coefficient

σ, specific heat C_p, thermal conductivity k and the small positive parameter related to the width of a diffusive interface ϵ. Considering the hybrid system (1), the total energy can be defined as:

$$E = \int_S \left(\frac{\rho |\mathbf{v}(\mathbf{x}, t)|^2}{2} + \rho \left(\frac{\sigma \epsilon}{2} |\nabla_S \phi(\mathbf{x}, t)|^2 + \frac{\sigma}{\epsilon} f(\phi(\mathbf{x}, t)) \right) + \frac{\rho C_p T^2}{2} \right) d\mathbf{x}, \tag{2}$$

which satisfies the following energy dissipation law:

$$\begin{aligned}
&\frac{d}{dt} E(\phi, \mathbf{v}, T) \\
&= \int_\Omega \rho \left(\mathbf{v}, \mathbf{v}_t\right) + \rho\sigma\epsilon \left(\nabla_S \phi, \nabla_S \phi_t\right) + \frac{\rho\sigma}{\epsilon} \left(f'(\phi), \phi_t\right) + \rho C_p \left(T, T_t\right) d\mathbf{x} \\
&= \int_\Omega \rho \left(\mathbf{v}, -\nabla_S p + \nabla_S \cdot (\eta \nabla_S \mathbf{v}) - \frac{\sigma}{\epsilon} \phi \nabla_S \mu - \rho \left(\frac{\mathbf{v} \cdot \nabla_S \mathbf{v}}{2} + \frac{\nabla_S \cdot (\mathbf{v} \otimes \mathbf{v})}{2} \right) \right) \\
&\quad + \frac{\rho\sigma}{\epsilon} \left(f'(\phi) - \epsilon^2 \Delta_S \phi, \phi_t \right) + \rho C_p \left(T, \frac{1}{\rho C_p} \nabla_S \cdot (k \nabla_S T) - \mathbf{v} \cdot \nabla_S T \right) d\mathbf{x} \\
&= \int_\Omega -\rho\eta |\nabla_S \mathbf{v}|^2 - \frac{\rho\sigma}{\epsilon} \left(\nabla_S \mu, \phi \mathbf{v}\right) + \frac{\rho\sigma}{\epsilon} (\mu, \phi_t) + \rho C_p \left(T, \frac{1}{\rho C_p} \nabla_S \cdot (k \nabla_S T) \right) d\mathbf{x} \\
&= \int_\Omega -\eta\rho |\nabla_S \mathbf{v}|^2 + \frac{\rho\sigma}{\epsilon} \left(\nabla_S \cdot (\phi \mathbf{v}), \mu \right) + \frac{\rho\sigma}{\epsilon} \left(\frac{1}{Pe} \Delta_S \mu - \nabla_S \cdot (\phi \mathbf{v}), \mu \right) - k |\nabla_S T|^2 d\mathbf{x} \\
&= \int_\Omega -\eta\rho |\nabla_S \mathbf{v}|^2 - \frac{\sigma\rho}{\epsilon Pe} |\nabla_S \mu|^2 - k |\nabla_S T|^2 d\mathbf{x} \le 0,
\end{aligned} \tag{3}$$

where the following identities have been used:

$$\begin{cases}
\left(\mathbf{v}, \nabla_S p\right) = -\left(\nabla_S \cdot \mathbf{v}, p\right) = 0, \\
\left(\mathbf{v}, \dfrac{\mathbf{v} \cdot \nabla_S \mathbf{v}}{2} + \dfrac{\nabla_S \cdot (\mathbf{v} \otimes \mathbf{v})}{2} \right) = 0, \\
\left(T, \mathbf{v} \cdot \nabla_S T\right) = 0.
\end{cases} \tag{4}$$

Remark 1. Let us introduce the following linear forms in the multiphysical system, i.e.,

$$\mathrm{B}(\mathbf{u}, v, w) = \frac{1}{2} \int_\Omega (\mathbf{u} \cdot (w \nabla v) - \mathbf{u} \cdot (v \nabla w)) dx, \tag{5}$$

$$\mathrm{B}(\mathbf{u}, \mathbf{v}, \mathbf{w}) = \frac{1}{2} \int_\Omega ((\mathbf{u} \cdot \nabla \mathbf{v}) \mathbf{w} - (\mathbf{u} \cdot \nabla \mathbf{w}) \mathbf{v}) dx + \frac{1}{2} \int_{\partial\Omega} \left((\mathbf{u} \cdot \mathbf{w}) (\mathbf{v} \cdot \mathbf{n}) - (\mathbf{u} \cdot \mathbf{v}) (\mathbf{w} \cdot \mathbf{n}) \right) dS. \tag{6}$$

The trilinear terms $\mathrm{B}(\mathbf{u}, v, w)$ and $\mathrm{B}(\mathbf{u}, \mathbf{v}, \mathbf{w})$ are the weak form of antisymmetric formulation of the advection term of the CH equations(Eqs. (1a), (1b)), Heat transfer equation(Eq. (1e)), and NS equations(Eqs. (1c) and (1d)), respectively. Thus, the following identity can be obtained

$$B(\mathbf{u}, v, v) = 0, \quad \text{and} \quad B(\mathbf{u}, \mathbf{v}, \mathbf{v}) = 0. \tag{7}$$

The detailed proof can be found in Ref. [36]. It should be emphasized that these identities hold regardless of whether $\mathbf{u}$ and $\mathbf{v}$ are divergence free or not, which is helpful to preserve the stability.

The coupling system over arbitrary manifolds can yield rich applications, such as simulation of wildland fire [37], organization in alloy electrodeposition [38] and face recognition [39]. However, the major problem with these kinds of applications is the handling of the coupling relationships. The solution system is transformed from the original two-dimensional space to three-dimensional space, which makes computational cost increase geometrically because of the existence of the coupling term [40]. The introduction of multi-coupling to the system makes the solution difficult to converge, while the high accuracy of the original simple system is not guaranteed [41–43].

3. Numerical scheme for the binary thermal fluids system on arbitrary surfaces

Let us first introduce the discrete formulation and implementation for the proposed hybrid system. The thermodynamic scheme is discretized on the triangular surface mesh $\Sigma := (P, T)$. Here, $P = \{\mathbf{p}_i | 1 \le i \le N_P\}$ denotes the set of N_P vertices and $T = \{T_i | 1 \le i \le N_T\}$ denotes the set of N_T triangles. As shown in Fig. 1, we mark the vertices as red circle and the triangles as blue faces. Let us consider the one-ring neighbors of the vertex $\mathbf{p} \in P$. By assuming that there are s vertices around $\mathbf{p}$, for $j = 1, 2, \ldots, s$, $\mathbf{p}_j$ is counterclockwise oriented and $\mathbf{p}_{s+1} = \mathbf{p}_1$. Let us define triangle T_j with three vertices $\mathbf{p}$, $\mathbf{p}_j$ and $\mathbf{p}_{j+1}$, where $G_j = \left(\mathbf{p} + \mathbf{p}_j + \mathbf{p}_{j+1}\right)/3$ is the centroid of this triangle. Besides, we define $\mathbf{N}_j$ as the unit normal vector to the triangle T_j and $\mathbf{n}_\mathbf{p}(T_j, \mathbf{G}_j)$ is the unit outward normal vector of the edge $\overline{\mathbf{p}_j \mathbf{p}_{j+1}}$ at $\mathbf{G}_j$ of the triangle T_j. Furthermore,

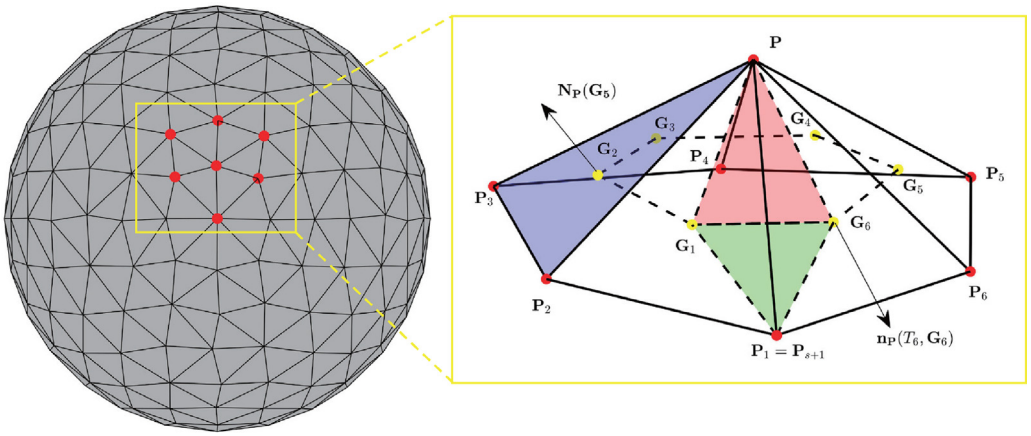

Fig. 1. Scheme illustration of the dual-mesh neighboring the vertex $\mathbf{p}$.

we define the local dual mesh as follows. Let the vertices $\mathbf{p}_j$, $\mathbf{G}_j$, $\mathbf{G}_{j+1}$ form a new triangle $\widetilde{T}_j$, which can be seen as the green triangle in Fig. 1. We define the union of the triangles $D_{\mathbf{p}} := \{\widetilde{T}_j | 1 \le j \le s\}$ as the local dual mesh of $\mathbf{p}$. Thus we can define the union of all local dual mesh $D_P := \{D_{\mathbf{p}} | \forall \mathbf{p} \in P\}$ as the dual mesh of the triangular mesh Σ.

Let ∇_h, $\nabla_h \cdot$ and Δ_h be the discrete gradient, divergence and Laplace–Beltrami operators, respectively. The definition of $\nabla_h X(\mathbf{G}_j)$ has second-order accuracy in space:

$$\nabla_h X(\mathbf{G}_j) = \alpha_j(\mathbf{p}_j - \mathbf{G}_j) + \beta_j(\mathbf{p}_{j+1} - \mathbf{G}_j). \tag{8}$$

where X is an arbitrary scalar-value function, α_j and β_j is the solution of the following equation:

$$\begin{pmatrix} \langle \mathbf{p}_j - \mathbf{G}_j, \mathbf{p} - \mathbf{G}_j \rangle & \langle \mathbf{p}_{j+1} - \mathbf{G}_j, \mathbf{p} - \mathbf{G}_j \rangle & \|\mathbf{p} - \mathbf{G}_j\|^2 \\ \langle \mathbf{p}_j - \mathbf{G}_j, \mathbf{p}_j - \mathbf{G}_j \rangle & \langle \mathbf{p}_{j+1} - \mathbf{G}_j, \mathbf{p}_j - \mathbf{G}_j \rangle & \|\mathbf{p}_j - \mathbf{G}_j\|^2 \\ \langle \mathbf{p}_j - \mathbf{G}_j, \mathbf{p}_{j+1} - \mathbf{G}_j \rangle & \langle \mathbf{p}_{j+1} - \mathbf{G}_j, \mathbf{p}_{j+1} - \mathbf{G}_j \rangle & \|\mathbf{p}_{j+1} - \mathbf{G}_j\|^2 \end{pmatrix} \begin{pmatrix} \alpha_j \\ \beta_j \\ 0.5\Delta_h X(\mathbf{G}_j) \end{pmatrix} = \begin{pmatrix} X(\mathbf{p}) - X(\mathbf{G}_j) \\ X(\mathbf{p}_j) - X(\mathbf{G}_j) \\ X(\mathbf{p}_{j+1}) - X(\mathbf{G}_j) \end{pmatrix}. \tag{9}$$

It should be remarked that the $\Delta_h X(\mathbf{G}_j)$ equals zero, which has been proved in Appendix. By using the Green function, the approximation of the Laplace–Beltrami operator can be defined as

$$\begin{aligned} \Delta_h X(\mathbf{p}) = \frac{1}{A(\mathbf{p})} \sum_{j=1}^{s+1} \frac{\|\mathbf{G}_{j+1} - \mathbf{G}_j\|}{6} \big(& 2\left\langle \nabla_h X(\mathbf{G}_j),\ \mathbf{n}_{\mathbf{p}}(T_j, \mathbf{G}_j) \right\rangle \\ & + 2\left\langle \nabla_h X(\mathbf{G}_{j+1}),\ \mathbf{n}_{\mathbf{p}}(T_j, \mathbf{G}_{j+1}) \right\rangle + \left\langle \nabla_h X(\mathbf{G}_j),\ \mathbf{n}_{\mathbf{p}}(T_j, \mathbf{G}_{j+1}) \right\rangle \\ & + \left\langle \nabla_h X(\mathbf{G}_{j+1}),\ \mathbf{n}_{\mathbf{p}}(T_j, \mathbf{G}_j) \right\rangle \big), \end{aligned} \tag{10}$$

where $A(\mathbf{p}) = \sum_{j=1}^{s+1} \left|\hat{T}_j\right|$ and $\left|\hat{T}_j\right|$ is the area of the triangle $\hat{T}_j$ with $\mathbf{p}$, $\mathbf{G}_j$ and $\mathbf{G}_{j+1}$, which remarked by the red triangle in Fig. 1. The outward normals $\mathbf{n}_{\mathbf{p}}(T_j, \mathbf{G}_j)$ and $\mathbf{n}_{\mathbf{p}}(T_j, \mathbf{G}_{j+1})$ are defined as

$$\mathbf{n}_{\mathbf{p}}(T_j, \mathbf{G}_j) = \frac{(\mathbf{G}_{j+1} - \mathbf{G}_j) \times \mathbf{N}_j}{\|(\mathbf{G}_{j+1} - \mathbf{G}_j) \times \mathbf{N}_j\|} \text{ and } \mathbf{n}_{\mathbf{p}}(T_j, \mathbf{G}_{j+1}) = \frac{(\mathbf{G}_{j+1} - \mathbf{G}_j) \times \mathbf{N}_{j+1}}{\|(\mathbf{G}_{j+1} - \mathbf{G}_j) \times \mathbf{N}_{j+1}\|}. \tag{11}$$

We should note that the outward normal vectors are defined on the lifting geodesic of $\overline{\mathbf{G}_j\mathbf{G}_{j+1}}$, which has been approximately computed over the edge $\overline{\mathbf{G}_j\mathbf{G}_{j+1}}$. As can be seen from Eq. (10), the discrete Laplace–Beltrami operator is second-order accurate since $\nabla_h X(\mathbf{G}_j)$ is provable to be second-order accurate in Eq. (8). In the same manner, we can define the second-order accurate discrete divergence operator as:

$$\begin{aligned} \nabla_h \cdot \mathbf{X}(\mathbf{p}) = \frac{1}{A(\mathbf{p})} \sum_{j=1}^{s+1} \frac{\|\mathbf{G}_{j+1} - \mathbf{G}_j\|}{6} \big(& 2\left\langle \mathbf{X}(\mathbf{G}_j),\ \mathbf{n}_{\mathbf{p}}(T_j, \mathbf{G}_j) \right\rangle \\ & + 2\left\langle \mathbf{X}(\mathbf{G}_{j+1}),\ \mathbf{n}_{\mathbf{p}}(T_j, \mathbf{G}_{j+1}) \right\rangle + \left\langle \mathbf{X}(T_j, \mathbf{G}_j),\ \mathbf{n}_{\mathbf{p}}(\mathbf{G}_{j+1}) \right\rangle + \left\langle \mathbf{X}(\mathbf{G}_{j+1}),\ \mathbf{n}_{\mathbf{p}}(T_j, \mathbf{G}_j) \right\rangle \big), \end{aligned} \tag{12}$$

where $\mathbf{X}$ is an arbitrary vector-value function. Based on the definition of the dual mesh, we can define the discrete gradient operator with the other discrete operators. Using the second-order Taylor expansion, we have

$$\begin{cases} X(\mathbf{p}) - X(\mathbf{G}_j) = \langle \nabla_h X(\mathbf{G}_j), \mathbf{p} - \mathbf{G}_j \rangle + 0.5 \Delta_h X(\mathbf{G}_j) \|\mathbf{p} - \mathbf{G}_j\|^2, \\ X(\mathbf{G}_j) - X(\mathbf{p}) = \langle \nabla_h X(\mathbf{p}), \mathbf{G}_j - \mathbf{p} \rangle + 0.5 \Delta_h X(\mathbf{p}) \|\mathbf{G}_j - \mathbf{p}\|^2. \end{cases} \tag{13}$$

By adding both the sides of the two equations in Eq. (13), we obtain

$$\langle \nabla_h X(\mathbf{p}), \mathbf{G}_j - \mathbf{p} \rangle = \langle \nabla_h X(\mathbf{G}_j), \mathbf{G}_j - \mathbf{p} \rangle - 0.5 \Delta_h X(\mathbf{p}) \|\mathbf{G}_j - \mathbf{p}\|^2. \tag{14}$$

Therefore, the discrete gradient operator can be defined as

$$\nabla_h X(\mathbf{p}) = \sum_{j=1}^{s+1} \frac{\|\mathbf{G}_j - \mathbf{p}\|^{-2}}{\sum_{k=1}^{s+1} \|\mathbf{G}_k - \mathbf{p}\|^{-2}} \nabla_h X(\mathbf{G}_j) - \sum_{j=1}^{s+1} \frac{\|\mathbf{G}_j - \mathbf{p}\|^{-2}}{2 \sum_{k=1}^{s+1} \|\mathbf{G}_k - \mathbf{p}\|^{-2}} \Delta_h X(\mathbf{p})(\mathbf{G}_j - \mathbf{p}). \tag{15}$$

Note that Eq. (15) is spatially second-order accurate because $\nabla_h X(\mathbf{G}_j)$ and $\Delta_h X(\mathbf{p})$ are provable to be second-order accurate. Herein, the discrete operators used in our proposed system have been defined with spatially second-order accuracy.

3.1. Second-order accurate discrete system

Let us first define the discrete inner products on surfaces to support the subsequent proofs of energy dissipation. If ϕ_i and ψ_i are the functions on surfaces $\phi_i := \phi(\mathbf{p}_i)$ and $\psi_i := \psi(\mathbf{p}_i)$, the discrete inner product is

$$(\phi, \psi)_h := \sum_{\mathbf{p}_i \in P} \phi_i \psi_i A(\mathbf{p}_i), \quad (\nabla_h \phi, \nabla_h \psi)_h := \sum_{\mathbf{p}_i \in P} \left(A(\mathbf{p}_i) \sum_{j=0}^{s-1} \nabla_h \phi(\mathbf{G}_j) \cdot \nabla_h \psi(\mathbf{G}_j) \right), \tag{16}$$

the discrete norm is $\|\phi\|_h^2 = (\phi, \phi)_h$ and $\|\nabla_h \phi\|_h^2 = (\nabla_h \phi, \nabla_h \phi)_h$. We present the second-order numerical scheme for the thermodynamical flow on surfaces with the Crank–Nicolson-type formulation based on Eq. (1):

$$\frac{\phi_i^{n+1} - \phi_i^n}{\Delta t} + \nabla_h \cdot \left(\widetilde{\phi}_i^{n+\frac{1}{2}} \left(\frac{1}{2} \mathbf{v}_i^* + \frac{1}{2} \mathbf{v}_i^n \right) \right) = \frac{1}{Pe} \Delta_h \mu_i^{n+\frac{1}{2}}, \tag{17a}$$

$$\mu_i^{n+\frac{1}{2}} = \frac{f(\phi_i^{n+1}) - f(\phi_i^n)}{\phi_i^{n+1} - \phi_i^n} - \epsilon^2 \Delta_h \frac{\phi_i^{n+1} + \phi_i^n}{2}, \tag{17b}$$

$$\begin{aligned} \rho \frac{\mathbf{v}_i^* - \mathbf{v}_i^n}{\Delta t} + \frac{\rho}{2} \left(\widetilde{\mathbf{v}}_i^{n+\frac{1}{2}} \cdot \nabla_h (\frac{1}{2} \mathbf{v}_i^* + \frac{1}{2} \mathbf{v}_i^n) + \nabla_h \cdot \left(\widetilde{\mathbf{v}}_i^{n+\frac{1}{2}} \otimes (\frac{1}{2} \mathbf{v}_i^* + \frac{1}{2} \mathbf{v}_i^n) \right) \right) \\ = -\nabla_h p_i^n + \nabla_h \cdot \left(\eta \nabla_h (\frac{1}{2} \mathbf{v}_i^* + \frac{1}{2} \mathbf{v}_i^n) \right) - \frac{\sigma}{\epsilon} \widetilde{\phi}_i^{n+\frac{1}{2}} \nabla_h \mu_i^{n+\frac{1}{2}}, \end{aligned} \tag{17c}$$

$$\rho \frac{\mathbf{v}_i^{n+1} - \mathbf{v}_i^*}{\Delta t} + \frac{1}{2} \nabla_h \left(p_i^{n+1} - p_i^n \right) = 0, \tag{17d}$$

$$\nabla_h \cdot \mathbf{v}_i^{n+1} = 0, \tag{17e}$$

$$\rho C_p \left(\frac{T_i^{n+1} - T_i^n}{\Delta t} \right) = \nabla_h \cdot (k \nabla_h T_i^{n+\frac{1}{2}}) - \rho C_p \mathbf{v}_i^{n+\frac{1}{2}} \cdot \nabla_h T_i^{n+\frac{1}{2}}, \tag{17f}$$

where $\widetilde{\mathbf{v}}_i^{n+\frac{1}{2}} = 1.5\mathbf{v}_i^n - 0.5\mathbf{v}_i^{n-1}$, $\mathbf{v}_i^{n+\frac{1}{2}} = 0.5\mathbf{v}_i^{n+1} + 0.5\mathbf{v}_i^n$ and $\mathbf{v}_i^*$ is the intermediate velocity of the projection method. Then, we describe the computational solutions of the proposed thermodynamical fluid system. Since the three physical fields, i.e., the phase field, velocity field and the temperature field, are strongly coupled with each other, we should solve the complicated system in a temporally matched manner. For the given initial ϕ^n, $\mathbf{u}^n$ and T^n, we want to compute ϕ^{n+1}, $\mathbf{u}^{n+1}$ and T^{n+1} with the following steps:

Step 1. Given the initial $\mathbf{v}_i^{n-1}$, $\mathbf{v}_i^n$, ϕ_i^{n-1} and ϕ_i^n, we want to find ϕ_i^{n+1} and $\mu_i^{n+\frac{1}{2}}$ with Eqs. (17a) and (17b) by the following equations

$$\begin{cases} \dfrac{\phi_i^{n+1,m+1} - \phi_i^n}{\Delta t} + \nabla_h \cdot \left(\widetilde{\phi}_i^{n+\frac{1}{2}} \left(\dfrac{1}{2} \mathbf{v}_i^* + \dfrac{1}{2} \mathbf{v}_i^n \right) \right) = \dfrac{1}{2Pe} \Delta_h \left(\mu_i^{n+1,m+1} + \mu_i^n \right), \\ \dfrac{\mu_i^{n+1,m+1} + \mu_i^n}{2} = g(\phi_i^{n+1}, m) - \epsilon^2 \dfrac{\Delta_h \phi_i^{n+1,m+1} + \Delta_h \phi_i^n}{2}, \end{cases} \tag{18}$$

where $g(\phi_i^{n+1,m}) := (f(\phi_i^{n+1,m}) - f(\phi_i^n))/(\phi_i^{n+1,m} - \phi_i^n)$ is the discrete chemical potential and m is the index of Picard iteration. This step is executed until the relative error is smaller than a give tolerance *tol* as:

$$\left\| \phi_i^{n+1,m} - \phi_i^{n+1,m-1} \right\|_h \leq tol. \tag{19}$$

Then, we set $\phi_i^{n+1} = \phi_i^{n+1,m+1}$. The initial condition $\phi_i^{n+1,0}$ is defined as $\phi_i^{n+1,0} = 2\phi_i^n - \phi_i^{n-1}$. For the first loop $n = 1$, we use $\mathbf{v}_i^* = \mathbf{v}_i^1$. In addition, we choose the $\mathbf{v}_i^*$ as the solved intermediate velocity at the last time step. The discrete CH equation can be efficiently solved by a biconjugate gradient stabilized method and the residual error converges rather quickly to the given tolerance $tol = 1e-6$ with few iterations.

Step 2. With the given p_i^n, $\mathbf{v}_i^n$ and $\widetilde{\phi}_i^{n+\frac{1}{2}}$, we update the intermediate velocity $\mathbf{v}_i^*$ with Eq. (17c) as

$$\begin{aligned}\left(\mathcal{I} - \frac{\Delta t\eta}{2\rho}\Delta_h\right)\mathbf{v}_i^* = &-\Delta t\left(\widetilde{\mathbf{v}}_i^{n+\frac{1}{2}}\cdot\nabla_h\widetilde{\mathbf{v}}_i^* + \nabla_h\cdot\left(\widetilde{\mathbf{v}}_i^{n+\frac{1}{2}}\otimes(\frac{1}{2}\mathbf{v}_i^* + \frac{1}{2}\mathbf{v}_i^n)\right)\right)\\ &+\frac{\Delta t}{\rho}\left(-\nabla_h p_i^n + \frac{\eta}{2}\Delta_h\mathbf{v}_i^n - \frac{\sigma\widetilde{\phi}_i^{n+\frac{1}{2}}}{2\epsilon}\nabla_h\mu_i^{n+\frac{1}{2}}\right) + \mathbf{v}_i^n,\end{aligned} \tag{20}$$

where $\mathcal{I}$ denotes the identity matrix. The Adams–Bashforth extrapolation has been used to solve the convection term explicitly. Furthermore, we applied the biconjugate gradient stabilized method in this step.

Step 3. By taking the divergence operator to both the sides of Eq. (17d), we solve the Poisson-type equation as:

$$\Delta_h p_i^{n+1,m+1} + Dp_i^{n+1,m+1} = \Delta_h p_i^n + Dp_i^{n+1,m} + \frac{2\rho}{\Delta t}\nabla_h\cdot\mathbf{v}_i^*, \tag{21}$$

where $(\Delta_h + D)$ is a diagonally dominant matrix. In this paper, we choose $D = 0.01\mathcal{I}$. The indicator m is the index of the Picard iteration. We apply this step until the convergence condition is satisfied with the given tolerance as:

$$\left\|p_i^{n+1,m+1} - p_i^{n+1,m}\right\|_h \le tol. \tag{22}$$

Thus, we set $p_i^{n+1} = p_i^{n+1,m+1}$ with the initial condition $p_i^{n+1,0} = 2p_i^n - p_i^{n-1}$.

Step 4. By updating the velocity field with Eq. (17d) we can obtain:

$$\mathbf{v}_i^{n+1} = \frac{\Delta t}{2\rho}\nabla_h\left(p_i^n - p_i^{n+1}\right) + \mathbf{v}_i^*. \tag{23}$$

Step 5. With the given T_i^n, $\mathbf{v}_i^n$ and the updated velocity field $\mathbf{v}_i^{n+1}$, we can obtain

$$\left(\rho C_p\mathcal{I} - \frac{\Delta tk}{2}\Delta_h\right)T_i^{n+1,m+1} = \left(\rho C_p\mathcal{I} + \frac{\Delta tk}{2}\Delta_h\right)T_i^n - \Delta t\rho C_p\mathbf{v}_i^{n+\frac{1}{2}}\cdot\nabla_h\frac{T_i^{n+1,m} + T_i^n}{2}, \tag{24}$$

where m is the index of the Picard iteration. Similarly as Step 1 and 2, we still use the efficient biconjugate method and terminate the procedure if the truncation error satisfies: $\left\|T_i^{n+1,m+1} - T_i^{n+1,m}\right\|_h \le tol$. Thus, we set $T_i^{n+1} = T_i^{n+1,m+1}$ with the initial condition $T_i^{n+1,0} = 2T_i^n - T_i^{n-1}$.

Some remarks should be summarized here: (i) Our proposed scheme Eq. (17) is a three-level scheme that requires setting initial step ϕ_i^{-1}, $\mathbf{v}_i^{-1}$ and T_i^{-1} to guarantee second-order accuracy for every time step. In this study, $\phi_i^{-1} := \phi_i^0$, $\mathbf{v}_i^{-1} := \mathbf{v}_i^0$ and $T_i^{-1} := T_i^0$ is simple, but lowers the accuracy in the first time step, which has been proved in [44] to investigate that the accuracy is sensitive to the initial value. However, our scheme is indeed second-order accurate for later calculations. Therefore, for a lengthy simulation, second-order accuracy with respect to time and space can be observed. (ii) The proposed method is directly applied for the formulation on arbitrary surfaces, which provides the possibility of computation for coupling multiple physical fields without additional complexity. (iii) Based on the Crank–Nicolson-type framework, the discrete energy dissipation law and mass conservative law are satisfied for arbitrary complex surfaces. (iv) The Picard iterations applied in this system is simple and robust, which makes the original nonlinear problem become a linear solvable problem and converge efficiently. (v) The second-order error analysis under the Crank–Nicolson framework is omitted, which can be refereed to [45,46] and yields to the same results without loss generality.

3.2. Unconditional stability for the numerical scheme

In this subsection, we prove the proposed method Eqs. (17) is unconditionally stable, which admits a unique solution for the hybrid system. Thus we give the following law of the energy dissipation:

Theorem 1. *The solutions of Eqs. (17) make the modified energy decay with respect to time, i.e.,*

$$\begin{aligned}&\left(E^{n+1} + \Delta t^2\|\nabla_h p^{n+1}\|_h^2/(8\rho)\right) - \left(E^n + \Delta t^2\|\nabla_h p^n\|_h^2/(8\rho)\right)\\ &= -\frac{\Delta t\eta}{4}\left\|\nabla_h(\mathbf{v}^* + \mathbf{v}^n)\right\|_h^2 - \frac{\rho\Delta t\sigma}{\epsilon Pe}\|\nabla_h\mu^{n+\frac{1}{2}}\|_h^2 - \Delta tk\left\|\nabla_h T^{n+\frac{1}{2}}\right\|_h^2 \le 0,\end{aligned} \tag{25}$$

where $E^n = \rho\|\mathbf{v}^n\|_h^2/2 + \rho\epsilon\sigma\|\nabla_h\phi^n\|_h^2/2 + \rho\sigma\left(f\left(\phi^n\right), 1\right)_h/\epsilon + \rho C_p(T^n)^2/2$ *is the total energy.*

Proof. Given total energy form of E^n, to prove energy decay, we need to deduce the energy dissipation with the discrete form can be expressed as follows:

$$\begin{aligned}
&\left(E^{n+1}+\Delta t^2\|\nabla_h p^{n+1}\|_h^2/(8\rho)\right)-\left(E^n+\Delta t^2\|\nabla_h p^n\|_h^2/(8\rho)\right)\\
&=\frac{\rho\left(\left\|\mathbf{v}^{n+1}\right\|_h^2-\|\mathbf{v}^n\|_h^2\right)}{2}-\Delta t\rho\sigma\epsilon\left(\Delta_h\phi^{n+\frac12},\phi_t^{n+\frac12}\right)_h\\
&+\frac{\Delta t\rho\sigma}{\epsilon}\left(\frac{f\left(\phi^{n+1}\right)-f\left(\phi^n\right)}{\phi^{n+1}-\phi^n},\phi_t^{n+\frac12}\right)_h+\frac{\Delta t^2}{8\rho}\left(\left\|\nabla_h p^{n+1}\right\|_h^2-\left\|\nabla_h p^n\right\|_h^2\right)+\left(\Delta t\rho C_pT^{n+\frac12},T_t^{n+\frac12}\right)\\
&=\frac{\rho\left(\left\|\mathbf{v}^{n+1}\right\|_h^2-\|\mathbf{v}^*\|_h^2\right)}{2}+\frac{\rho\left(\|\mathbf{v}^*\|_h^2-\|\mathbf{v}^n\|_h^2\right)}{2}\\
&+\frac{\Delta t\rho\sigma}{\epsilon}\left(\mu^{n+\frac12},\phi_t^{n+\frac12}\right)_h+\frac{\Delta t^2}{8\rho}\left(\left\|\nabla_h p^{n+1}\right\|_h^2-\left\|\nabla_h p^n\right\|_h^2\right)+\left(\Delta t\rho C_pT^{n+\frac12},T_t^{n+\frac12}\right).
\end{aligned}$$

By taking L_2 inner product of Eq. (17c) with $(\mathbf{v}^*+\mathbf{v}^n)\Delta t/(2\rho)$, we can have

$$\begin{aligned}
&\frac{\left(\|\mathbf{v}^*\|_h^2-\|\mathbf{v}^n\|_h^2\right)}{2\Delta t}\\
&=-\frac{1}{2\rho}\left(\nabla_h p^n,\mathbf{v}^*+\mathbf{v}^n\right)_h-\frac{\sigma}{2\epsilon}\left(\widetilde{\phi}^{n+\frac12}\nabla_h\mu^{n+\frac12},\mathbf{v}^*+\mathbf{v}^n\right)_h-\frac{\eta}{4\rho}\left\|\nabla_h(\mathbf{v}^*+\mathbf{v}^n)\right\|_h^2.
\end{aligned}\tag{26}$$

By considering the identity Eq. (6) of the trilinear form from [36], we can obtain

$$\begin{aligned}
&\left(\mathbf{v}^*+\mathbf{v}^n,\widetilde{\mathbf{v}}^{n+\frac12}\cdot\nabla_h(\mathbf{v}^*+\mathbf{v}^n)+\nabla_h\cdot\left(\widetilde{\mathbf{v}}^{n+\frac12}(\mathbf{v}^*+\mathbf{v}^n)\right)\right)_h\\
&=\left((\mathbf{v}^*+\mathbf{v}^n)\widetilde{\mathbf{v}}^{n+\frac12},\nabla_h(\mathbf{v}^*+\mathbf{v}^n)\right)_h+\left(\mathbf{v}^*+\mathbf{v}^n,\nabla_h\cdot\left(\widetilde{\mathbf{v}}^{n+\frac12}(\mathbf{v}^*+\mathbf{v}^n)\right)\right)_h=0.
\end{aligned}\tag{27}$$

In order to derive the following equation:

$$\frac12\left(\left\|\mathbf{v}^{n+1}\right\|_h^2-\left\|\mathbf{v}^*\right\|_h^2\right)=-\frac12\left\|\mathbf{v}^{n+1}-\mathbf{v}^*\right\|_h^2=-\frac{\Delta t^2}{8\rho^2}\left\|\nabla_h\left(p^{n+1}-p^n\right)\right\|_h^2.$$

We take the L_2 inner product of Eq. (17d) with $\mathbf{v}^{n+1}\Delta t/\rho$, which leads to:

$$\left(\mathbf{v}^{n+1},\mathbf{v}^{n+1}-\mathbf{v}^*\right)_h=-\frac{\Delta t}{2\rho}\left(\nabla_h\left(p^{n+1}-p^n\right),\mathbf{v}^{n+1}\right)_h=\frac{\Delta t}{2\rho}\left(\left(p^{n+1}-p^n\right),\nabla_h\cdot\mathbf{v}^{n+1}\right)_h=0.$$

Rewriting the projection step of Eq. (17d) as

$$\frac{\left(\mathbf{v}^{n+1}+\mathbf{v}^n\right)-\left(\mathbf{v}^*+\mathbf{v}^n\right)}{\Delta t}+\frac{1}{2\rho}\nabla_h\left(p^{n+1}-p^n\right)=0.\tag{28}$$

Then, by taking L_2 inner product with $\Delta t^2\nabla_h p^n/2$, we have

$$\frac{\Delta t^2}{8}\left\|\nabla_h\left(p^{n+1}-p^n\right)\right\|_h^2=\frac{\Delta t^2}{8}\left(\left\|\nabla_h p^{n+1}\right\|_h^2-\left\|\nabla_h p^n\right\|_h^2\right)-\frac{\rho\Delta t}{2}\left(\nabla_h p^n,\mathbf{v}^*+\mathbf{v}^n\right)_h.\tag{29}$$

By multiplying Eq. (17a) with $\mu^{n+\frac12}$, using $\phi_t^{n+\frac12}=\left(\phi^{n+1}-\phi^n\right)/\Delta t$, we get

$$\left(\mu^{n+\frac12},\phi_t^{n+\frac12}\right)_h=-\frac{1}{Pe}\left\|\nabla_h\mu^{n+\frac12}\right\|_h^2-\frac12\left(\mu^{n+\frac12},\nabla_h\cdot\left(\widetilde{\phi}^{n+\frac12}(\mathbf{v}^*+\mathbf{v}^n)\right)\right)_h.\tag{30}$$

Similarly, by taking L_2 inner product of Eq. (17f) with $\Delta t\rho C_pT^{n+\frac12}$ and using the identity Eq. (5) from [36], we have

$$\begin{aligned}
&\left(\Delta t\rho C_pT^{n+\frac12},T_t^{n+\frac12}\right)_h\\
&=\left(\Delta t\rho C_pT^{n+\frac12},\frac{1}{\rho C_p}\nabla_h\cdot\left(k\nabla_hT^{n+\frac12}\right)-\mathbf{v}^{n+\frac12}\cdot\nabla_hT^{n+\frac12}\right)_h\\
&=\left(\Delta t\rho C_pT^{n+\frac12},\rho C_p\nabla_h\cdot\left(k\nabla_hT^{n+\frac12}\right)\right)_h-\left(\Delta t\rho C_pT^{n+\frac12},\mathbf{v}^{n+\frac12}\cdot\nabla_hT^{n+\frac12}\right)_h\\
&=\left(\Delta t\rho C_pT^{n+\frac12},\rho C_p\nabla_h\cdot\left(k\nabla_hT^{n+\frac12}\right)\right)_h+\left(\Delta t\rho C_pT^{n+\frac12},\left(\nabla_h\cdot\mathbf{v}^{n+\frac12}\right)\cdot T^{n+\frac12}\right)_h\\
&=-\frac{\Delta t\rho C_pk}{\rho C_p}\left(\nabla_hT^{n+\frac12},\nabla_hT^{n+\frac12}\right)_h=-\Delta tk\left\|\nabla_hT^{n+\frac12}\right\|_h^2.
\end{aligned}$$

In the end, we get the energy dissipation with the discrete form

$$\begin{aligned}&\left(E^{n+1}+\Delta t^2\|\nabla_h p^{n+1}\|_h^2/(8\rho)\right)-\left(E^n+\Delta t^2\|\nabla_h p^n\|_h^2/(8\rho)\right)\\&=-\frac{\Delta t\eta}{4}\left\|\nabla_h(\mathbf{v}^*+\mathbf{v}^n)\right\|_h^2-\frac{\rho\Delta t\sigma}{\epsilon Pe}\|\nabla_h\mu^{n+\frac{1}{2}}\|_h^2-\Delta tk\left\|\nabla_h T^{n+\frac{1}{2}}\right\|_h^2\le 0,\end{aligned}\tag{31}$$

by multiplying Eqs. (26) and (30) by $1/\Delta t$ and summing the results with $\Delta t\left(\left\|\nabla_h p^{n+1}\right\|_h^2-\|\nabla_h p^n\|_h^2\right)/8$ and $\left(\mu^{n+\frac{1}{2}},\ \phi_t^{n+\frac{1}{2}}\right)_h$. This completes the proof. □

3.3. Total mass conservation of the proposed system

In this subsection, we prove the total mass conservation for the discrete system, which corresponds to the physical context.

Theorem 2. *The total mass conservation law can be satisfied during the computation as:*

$$\sum_{\mathbf{p}_i\in P}\phi_i^{n+1}A(\mathbf{p}_i)=\sum_{\mathbf{p}_i\in P}\phi_i^{n}A(\mathbf{p}_i)=\cdots=\sum_{\mathbf{p}_i\in P}\phi_i^{1}A(\mathbf{p}_i)=\sum_{\mathbf{p}_i\in P}\phi_i^{0}A(\mathbf{p}_i).\tag{32}$$

Proof. Let us first introduce a notation for the dual mesh. All vertices are labeled counterclockwise, which implies that we can convert Eq. (11) as

$$\begin{cases}\mathbf{n}_{\mathbf{p}_{j+1}}(T_j,\mathbf{G}_j)=\dfrac{(\mathbf{G}_j-\mathbf{G}_{j+1})\times\mathbf{N}_j}{\|(\mathbf{G}_j-\mathbf{G}_{j+1})\times\mathbf{N}_j\|}=-\mathbf{n}_{\mathbf{p}}(T_j,\mathbf{G}_j),\\ \mathbf{n}_{\mathbf{p}_{j+1}}(T_j,\mathbf{G}_{j+1})=\dfrac{(\mathbf{G}_j-\mathbf{G}_{j+1})\times\mathbf{N}_{j+1}}{\|(\mathbf{G}_j-\mathbf{G}_{j+1})\times\mathbf{N}_{j+1}\|}=-\mathbf{n}_{\mathbf{p}}(T_j,\mathbf{G}_{j+1}),\end{cases}\tag{33}$$

which is evident in the example of the red and green dual mesh in Fig. 1. Thus, we consider $\sum_{\mathbf{p}_i\in P}\phi_i^{n+1}A(\mathbf{p}_i)=\sum_{\mathbf{p}_i\in P}\phi_i^{n}A(\mathbf{p}_i)$ by multiplying the equality with $A(\mathbf{p})$ and summing by parts. The following equation can be obtained as:

$$\begin{aligned}&\sum_{\mathbf{p}_i\in P}\phi_i^{n+1}A(\mathbf{p}_i)-\sum_{\mathbf{p}_i\in P}\phi_i^{n}A(\mathbf{p}_i)\\&=\Delta t\sum_{\mathbf{p}_i\in P}(\frac{\Delta_h\mu_i^{n+\frac{1}{2}}}{Pe}+\nabla_h\cdot(\widetilde{\phi}_i^{n+\frac{1}{2}}\hat{\mathbf{v}}_i^{n+\frac{1}{2}}))A(\mathbf{p}_i)\\&=\Delta t\sum_{\mathbf{p}_i\in P}\left(\sum_{j=0}^{s-1}\frac{\|\mathbf{G}_{j+1}-\mathbf{G}_j\|}{6}\left(2\left\langle(\frac{\nabla_h\mu^{n+\frac{1}{2}}}{Pe}+\widetilde{\phi}^{n+\frac{1}{2}}\hat{\mathbf{v}}^{n+\frac{1}{2}})(\mathbf{G}_j),\ \mathbf{n}(T_j,\mathbf{G}_j)\right\rangle\right.\right.\\&\quad+2\left\langle(\frac{\nabla_h\mu^{n+\frac{1}{2}}}{Pe}+\widetilde{\phi}^{n+\frac{1}{2}}\hat{\mathbf{v}}^{n+\frac{1}{2}})(\mathbf{G}_{j+1}),\ \mathbf{n}(T_j,\mathbf{G}_{j+1})\right\rangle\\&\quad+\left\langle(\frac{\nabla_h\mu^{n+\frac{1}{2}}}{Pe}+\widetilde{\phi}^{n+\frac{1}{2}}\hat{\mathbf{v}}^{n+\frac{1}{2}})(\mathbf{G}_j),\ \mathbf{n}(T_j,\mathbf{G}_{j+1})\right\rangle\\&\quad\left.\left.+\left\langle(\frac{\nabla_h\mu^{n+\frac{1}{2}}}{Pe}+\widetilde{\phi}^{n+\frac{1}{2}}\hat{\mathbf{v}}^{n+\frac{1}{2}})(\mathbf{G}_{j+1}),\ \mathbf{n}(T_j,\mathbf{G}_j)\right\rangle\right)\right)\\&=\Delta t\sum_{\overline{\mathbf{G}_j\mathbf{G}_{j+1}}\in\widetilde{P}}\left(\frac{\|\mathbf{G}_{j+1}-\mathbf{G}_j\|}{6}\left(2\left\langle(\frac{\nabla_h\mu^{n+\frac{1}{2}}}{Pe}+\widetilde{\phi}^{n+\frac{1}{2}}\hat{\mathbf{v}}^{n+\frac{1}{2}})(\mathbf{G}_j),\ \mathbf{n}_{\mathbf{p}}(T_j,\mathbf{G}_j)\right\rangle\right.\right.\\&\quad+2\left\langle(\frac{\nabla_h\mu^{n+\frac{1}{2}}}{Pe}+\widetilde{\phi}^{n+\frac{1}{2}}\hat{\mathbf{v}}^{n+\frac{1}{2}})(\mathbf{G}_{j+1}),\ \mathbf{n}_{\mathbf{p}}(T_j,\mathbf{G}_{j+1})\right\rangle\\&\quad+\left\langle(\frac{\nabla_h\mu^{n+\frac{1}{2}}}{Pe}+\widetilde{\phi}^{n+\frac{1}{2}}\hat{\mathbf{v}}^{n+\frac{1}{2}})(\mathbf{G}_j),\ \mathbf{n}_{\mathbf{p}}(T_j,\mathbf{G}_{j+1})\right\rangle\\&\quad\left.+\left\langle(\frac{\nabla_h\mu^{n+\frac{1}{2}}}{Pe}+\widetilde{\phi}^{n+\frac{1}{2}}\hat{\mathbf{v}}^{n+\frac{1}{2}})(\mathbf{G}_{j+1}),\ \mathbf{n}_{\mathbf{p}}(T_j,\mathbf{G}_j)\right\rangle\right.\end{aligned}$$

$$+2\left\langle (\frac{\nabla_h \mu^{n+\frac{1}{2}}}{Pe}+\widetilde{\phi}^{n+\frac{1}{2}}\hat{\mathbf{v}}^{n+\frac{1}{2}})(\mathbf{G}_j),\ \mathbf{n}_{\mathbf{p}_{j+1}}(T_j,\mathbf{G}_j)\right\rangle$$
$$+2\left\langle (\frac{\nabla_h \mu^{n+\frac{1}{2}}}{Pe}+\widetilde{\phi}^{n+\frac{1}{2}}\hat{\mathbf{v}}^{n+\frac{1}{2}})(\mathbf{G}_{j+1}),\ \mathbf{n}_{\mathbf{p}_{j+1}}(T_j,\mathbf{G}_{j+1})\right\rangle$$
$$+\left\langle (\frac{\nabla_h \mu^{n+\frac{1}{2}}}{Pe}+\widetilde{\phi}^{n+\frac{1}{2}}\hat{\mathbf{v}}^{n+\frac{1}{2}})(\mathbf{G}_j),\ \mathbf{n}_{\mathbf{p}_{j+1}}(T_j,\mathbf{G}_{j+1})\right\rangle$$
$$+\left\langle (\frac{\nabla_h \mu^{n+\frac{1}{2}}}{Pe}+\widetilde{\phi}^{n+\frac{1}{2}}\hat{\mathbf{v}}^{n+\frac{1}{2}})(\mathbf{G}_{j+1}),\ \mathbf{n}_{\mathbf{p}_{j+1}}(T_j,\mathbf{G}_j)\right\rangle\Big)\Big),$$

where $\overline{\mathbf{G}_j\mathbf{G}_{j+1}}$ is the edge of $\mathbf{G}_j\mathbf{G}_{j+1}\in\widetilde{P}$. By taking Eq. (33) into Eq. 2, we can directly obtain

$$\sum_{\mathbf{p}_i\in P}\phi_i^{n+1}A(\mathbf{p}_i)=\sum_{\mathbf{p}_i\in P}\phi_i^{n}A(\mathbf{p}_i).$$

Therefore, we have the chain of equalities

$$\sum_{\mathbf{p}_i\in P}\phi_i^{n+1}A(\mathbf{p}_i)=\sum_{\mathbf{p}_i\in P}\phi_i^{n}A(\mathbf{p}_i)=\cdots=\sum_{\mathbf{p}_i\in P}\phi_i^{1}A(\mathbf{p}_i)=\sum_{\mathbf{p}_i\in P}\phi_i^{0}A(\mathbf{p}_i),$$

which corresponds to Eq. (32) and we complete the proof. □

3.4. Unconditional unique solvability for the proposed scheme

In this subsection, we prove that the discrete scheme Eq. (17) is unconditionally solvable. We should emphasize that the velocity, pressure, chemical potential, and the phase field are coupled with each other, while the temperature field is 'one-way' coupled with the velocity field and the phase field, i.e. the temperature is influenced by the velocity and phase field function but the reverse is invalid. To prove the unconditionally unique solvability of the proposed scheme Eqs. (17), we should consider the weak form of the discrete system. We first make some notations: (i) The pressure equation Eqs. (17d) and (17e) are decoupled from Eqs. (17a)–(17c). (ii) We can find $\mathbf{u}^{n+1}$ and p^{n+1} by solving the Darcy problem with Eqs. (21) and (23). (iii) The heat transfer equation Eq. (17f) is decoupled from Eqs. (17a)–(17c), which can be strictly solved with the solution $\mathbf{v}^{n+\frac{1}{2}}$ of Eq. (17d) and (17e). (iv) With the given $\mathbf{v}^{n+\frac{1}{2}}$, the heat transfer equation Eq. (17f) is unconditionally unique solvable, which has been widely investigated in several studies [47,48] and we omit the details here for conciseness. Thus we only need to establish the unique solvability of Eqs. (17a)–(17c). Let us define the L^2 subspace with mean zero as $L_0^2(\Omega):=\left\{f\in L^2(\Omega);\int_\Omega f dx=0\right\}$. We first establish the weak form of Eqs. (17a)–(17c) as: With the given ϕ^n, $\phi^{n-1}\in H^1(\Omega)$, $p^n\in H^1(\Omega)\cap L_0^2(\Omega)$, and $\mathbf{u}^n$, $\mathbf{u}^{n-1}\in\mathbf{H}^1(\Omega)$, the triple $\{\phi^{n+1},\mu^{n+1},\mathbf{v}^{n+1}\}$ is the weak solution of Eqs. (17a)–(17c) if the following identities can be satisfied:

$$\left(\phi^{n+1}-\phi^n,\psi\right)+\frac{\Delta t}{Pe}\left(\nabla_h\mu^{n+\frac{1}{2}},\nabla_h\psi\right)-\frac{\Delta t}{2}\left(\widetilde{\phi}^{n+\frac{1}{2}}(\mathbf{v}^*+\mathbf{v}^n),\nabla_h\psi\right)=0,\quad\forall\psi\in H^1(\Omega),\tag{34}$$

$$\left(\mu^{n+\frac{1}{2}},\nu\right)=(g(\phi^{n+1}),\nu)+\frac{\epsilon^2}{2}\left(\nabla_h\left(\phi^{n+1}+\phi^n\right),\nabla_h\nu\right),\quad\forall\nu\in H^1(\Omega),\tag{35}$$

$$2\left((\mathbf{v}^*+\mathbf{v}^n)/2-\mathbf{v}^n,\mathbf{u}\right)+\Delta t\frac{\eta}{2}\left(\nabla_h(\mathbf{v}^*+\mathbf{v}^n),\nabla_h\mathbf{u}\right)+\Delta t\frac{\rho}{2}B\left(\widetilde{\mathbf{v}}^{n+\frac{1}{2}},(\mathbf{v}^*+\mathbf{v}^n)/2,\mathbf{u}\right)$$
$$=-\Delta t\left(\nabla_h p^n,\mathbf{u}\right)-\Delta t\frac{\sigma}{\epsilon}\left(\widetilde{\phi}^{n+\frac{1}{2}}\nabla_h\mu^{n+\frac{1}{2}},\mathbf{u}\right),\quad\forall\mathbf{u}\in\mathbf{H}_0^1(\Omega),\tag{36}$$

with $\phi^{n+1}\in H^1(\Omega)$, $\mu^{n+\frac{1}{2}}\in H^1(\Omega)$, $\mathbf{v}^*\in\mathbf{H}_0^1(\Omega)$. Thus we refer to [49] to established the unconditionally unique solvability based on the well-known Browder–Minty lemma in [50]. Before the unique solvable theorem, let us introduce three lemmas:

Lemma 1. *For the real and reflexive Banach space X, we denote the dual space of X as X', if we define the mappings $T:X\to X'$ is bounded, continuous, coercive and monotone, there exists a solution $u\in X$ for $T(u)=g$, $\forall g\in X'$. If the operator is strictly monotone, the solution $\mathbf{u}$ is unique. Equivalently, we use the coercivity of Browder–Minty lemma to identify the unique solvability of the solution:*

$$\lim_{\|u\|_X\to\infty}\frac{\langle T(u),u\rangle}{\|u\|_X}\to\infty.\tag{37}$$

Lemma 2. *There exists a unique solution $\phi^{n+1}\in H^1(\Omega)$ to weak from discrete equation Eq. (35) with the given chemical potential $\mu^{n+\frac{1}{2}}\in H^1(\Omega)$ and the know phase field variable ϕ^n, $\phi^{n-1}\in H^1(\Omega)$. In addition, the solution depends continuously on $\mu^{n+\frac{1}{2}}$ in the weak topology and is bounded.*

Remark 2. The boundedness and continuity of the solution readily follow from the fact that Eq. (35) is a semilinear elliptic equation for ϕ^{n+1} with cubic nonlinearity. We omit the details of proof for the conciseness.

Lemma 3. *There exists a unique solution $\mathbf{v}^* \in \mathbf{H}_0^1(\Omega)$ to weak from discrete equation Eq. (36) with the given chemical potential $\mu^{n+\frac{1}{2}} \in H^1(\Omega)$, the know phase field variable ϕ^n, $\phi^{n-1} \in H^1(\Omega)$, and the known $\mathbf{v}^n$, $\mathbf{v}^{n-1} \in \mathbf{H}^1$. In addition, the solution depends continuously on $\mu^{n+\frac{1}{2}}$ in the strong topology and is bounded.*

Remark 3. The boundedness and continuity of the solution for Eq. (36) can be proved by invoking the Lax–Milgram theorem [51]. We omit the details of proof for the conciseness.

Herein, we can give the unique solvability theorem:

Theorem 3. *With the known variables ϕ^n, $\phi^{n-1} \in H^1(\Omega)$, $\mathbf{v}^n$, $\mathbf{v}^{n-1} \in \mathbf{H}^1$, and $p^n \in H^1(\Omega)$, the discrete system Eqs. (17a)–(17c) is unconditionally solvable in the sense of Eqs. (34)–(36) with any time step-size $\Delta t > 0$.*

Proof. Let us defines an operator $\mathcal{G} : H^1(\Omega) \to (H^1(\Omega))'$ for any $\mu^{n+\frac{1}{2}} \in H^1(\Omega)$ such that

$$\langle \mathcal{G}(\mu^{n+\frac{1}{2}}), \nu\rangle := \left(\phi^{n+1} - \phi^n, \nu\right) + \frac{\Delta t}{Pe}(\nabla_h \mu^{n+\frac{1}{2}}, \nabla_h \nu) - \frac{\Delta t}{2}\left(\widetilde{\phi}^{n+\frac{1}{2}}(\mathbf{v}^* + \mathbf{v}^n), \nabla_h \nu\right), \quad \forall \nu \in H^1(\Omega). \tag{38}$$

Here we use $\langle\ ,\ \rangle$ to define the duality pairing between $(H^1(\Omega))'$ and $H^1(\Omega)$. The phase variable ϕ^{n+1} and $\mathbf{v}^*$ are unique solution of Eqs. (35) and (36), which are the straightforward results from Lemmas 2 and 3. Thus we establish the unique weak solvability by the following three steps.

$\mathcal{S}_1$: We can investigate the boundedness of the operator $\mathcal{G}$ as

$$|\langle \mathcal{G}(\mu^{n+\frac{1}{2}}), \nu\rangle| \le C(\Delta t)\left(\|\phi^{n+1}\|_{L^2} + \left\|\phi^n\right\|_{L^2} + \|\nabla \mu^{n+\frac{1}{2}}\|_{L^2} + \left\|\widetilde{\phi}^{n+\frac{1}{2}}\right\|_{H^1}\left\|\frac{\mathbf{v}^* + \mathbf{v}^n}{2}\right\|_{H^1}\right)\|\mathbf{u}\|_{H^1}, \tag{39}$$

which can be yielded from Lemmas 2 and 3. We use C to denote the constant may depend on Δt, ϵ, Ω, and $\|\phi^n\|_{H^1}$. In addition, the continuous property of the operator $\mathcal{G}$ can be obtained due to the continuity of ϕ^{n+1} and $\mathbf{v}^*$ in the same manner.

$\mathcal{S}_2$: We can derive the monotonicity based on the definition of $\mathcal{G}$ as

$$\begin{aligned}
&\langle \mathcal{G}(\mu^{n+\frac{1}{2}}) - \mathcal{G}(\nu), \mu^{n+\frac{1}{2}} - \nu\rangle \\
&= (\phi(\mu^{n+\frac{1}{2}}) - \phi(\nu), \mu^{n+\frac{1}{2}} - \nu) + \frac{\Delta t}{Pe}\left\|\nabla_h\left(\mu^{n+\frac{1}{2}} - \nu\right)\right\|_{L^2}^2 \\
&\quad - \frac{\Delta t}{2}\left(\widetilde{\phi}^{n+\frac{1}{2}}\left(\mathbf{v}^*\left(\mu^{n+\frac{1}{2}}\right) - \mathbf{v}^*(\nu)\right), \nabla_h\left(\mu^{n+\frac{1}{2}} - \nu\right)\right) \\
&= \frac{1}{4}\int_\Omega \left(\phi(\mu^{n+\frac{1}{2}}) - \phi(\nu)\right)\left((\phi(\mu^{n+\frac{1}{2}}) + \phi(\nu))^2 + \left(\phi(\mu^{n+\frac{1}{2}}) + \phi^n\right)^2 + \left(\phi^n + \phi(\nu)\right)^2\right)\Big(\phi(\mu^{n+\frac{1}{2}}) \\
&\quad - \phi(\nu)\Big)\, d\mathbf{x} + \frac{\epsilon^2}{2}\left(\nabla(\phi(\mu^{n+\frac{1}{2}}) - \phi(\nu)), \nabla(\phi(\mu^{n+\frac{1}{2}}) - \phi(\nu))\right) + \frac{\Delta t}{Pe}\left\|\nabla(\mu^{n+\frac{1}{2}} - \nu)\right\|_{L^2}^2 \\
&\quad + \frac{\epsilon}{\sigma}\left(2\|\mathbf{v}^*(\mu^{n+\frac{1}{2}}) - \mathbf{v}^*(\nu)\|_{L^2}^2 + \Delta t\eta\|\nabla(\mathbf{v}^*(\mu^{n+\frac{1}{2}}) - \mathbf{v}^*(\nu))\|_{L^2}^2\right) \ge 0.
\end{aligned} \tag{40}$$

We should make the following notations: (i) Here $\phi(\nu)$ is the solution to Eq. (35) and $\mathbf{v}^*(\nu)$ is the solution to Eq. (36) based on the given ν. (ii) The convective term vanishes thanks to the skew-symmetry. (iii) The equality can be obtain if only if $\mu^{n+\frac{1}{2}} = \nu$, which yields the strict monotonicity of the operator $\mathcal{G}$.

$\mathcal{S}_3$: We derive the coercivity of the operator $\mathcal{G}$. Let us consider

$$\begin{aligned}
&\langle T(\mu^{n+\frac{1}{2}}), \mu^{n+\frac{1}{2}}\rangle \\
&= \left(\phi^{n+1} - \phi^n, \mu^{n+\frac{1}{2}}\right) + \frac{\Delta t}{Pe}(\nabla_h \mu^{n+\frac{1}{2}}, \nabla_h \mu^{n+\frac{1}{2}}) - \frac{\Delta t}{2}\left(\widetilde{\phi}^{n+\frac{1}{2}}(\mathbf{v}^* + \mathbf{v}^n), \nabla_h \mu^{n+\frac{1}{2}}\right) \\
&= \int_\Omega \left(g(\phi^{n+1}), \phi^{n+1} - \phi^n\right) d\mathbf{x} + \frac{\epsilon^2}{2}\int_\Omega |\nabla_h \phi^{n+1}|^2 - \left|\nabla_h \phi^n\right|^2 d\mathbf{x} \\
&\quad + \frac{\Delta t}{Pe}(\nabla_h \mu^{n+\frac{1}{2}}, \nabla_h \mu^{n+\frac{1}{2}}) + \frac{\epsilon}{\sigma}\left(2\left\|\frac{\mathbf{v}^* + \mathbf{v}^n}{2}\right\|_{L^2}^2 + \Delta t\left\|\nabla_h\left(\frac{\mathbf{v}^* + \mathbf{v}^n}{2}\right)\right\|_{L^2}^2 - \Delta t\left(2\mathbf{v}^n - \nabla_h p^n, \frac{\mathbf{v}^* + \mathbf{v}^n}{2}\right)\right) \\
&\ge \int_\Omega \frac{1}{4}(\phi^{n+1})^4 - \frac{1}{4}(\phi^{n+1})^2 - (\phi^n)^2 d\mathbf{x} + \frac{\epsilon^2}{2}\int_\Omega |\nabla_h \phi^{n+1}|^2 - \left|\nabla_h \phi^n\right|^2 d\mathbf{x} \\
&\quad + C(\Delta t)\|\nabla_h \mu^{n+\frac{1}{2}}\|_{L^2}^2 + \frac{\epsilon}{\sigma}\left(2\left\|\frac{\mathbf{v}^* + \mathbf{v}^n}{2}\right\|_{L^2}^2 + \Delta t\left\|\nabla_h\left(\frac{\mathbf{v}^* + \mathbf{v}^n}{2}\right)\right\|_{L^2}^2 - \Delta t\left(2\mathbf{v}^n - \nabla_h p^n, \frac{\mathbf{v}^* + \mathbf{v}^n}{2}\right)\right)
\end{aligned}$$

$$
\begin{aligned}
&\geq \frac{1}{4}\int_{\Omega}(\phi^{n+1})^4 d\mathbf{x} + \frac{\epsilon^2}{2}\int_{\Omega}|\nabla_h\phi^{n+1}|^2 d\mathbf{x} - \frac{1}{4}\|\phi^{n+1}\|_{L_2}^2 - C(\epsilon)\left\|\phi^n\right\|_{H^1}^2 \\
&\quad + C(\Delta t)\|\nabla_h\mu^{n+\frac{1}{2}}\|_{L^2}^2 + \frac{\epsilon}{\sigma}\left(2\left\|\frac{\mathbf{v}^*+\mathbf{v}^n}{2}\right\|_{L^2}^2 + \Delta t\left\|\nabla_h\left(\frac{\mathbf{v}^*+\mathbf{v}^n}{2}\right)\right\|_{L^2}^2 - \Delta t\left(2\mathbf{v}^n - \nabla_h p^n, \frac{\mathbf{v}^*+\mathbf{v}^n}{2}\right)\right) \\
&\geq \frac{1}{4}\int_{\Omega}(\phi^{n+1})^4 d\mathbf{x} + \frac{\epsilon^2}{2}\int_{\Omega}|\nabla_h\phi^{n+1}|^2 d\mathbf{x} - \frac{1}{8}\|\phi^{n+1}\|_{L_4}^4 - \frac{1}{8}|\Omega| - C(\epsilon)\left\|\phi^n\right\|_{H^1}^2 + C(\Delta t)\|\nabla_h\mu^{n+\frac{1}{2}}\|_{L^2}^2 \\
&\quad + C(\epsilon,\sigma,\Delta t)\left(\left\|\frac{\mathbf{v}^*+\mathbf{v}^n}{2}\right\|_{L^2}^2 + \left\|\nabla_h\left(\frac{\mathbf{v}^*+\mathbf{v}^n}{2}\right)\right\|_{L^2}^2 - \left(\left\|\mathbf{v}^n\right\|_{L^2}^2 + \left\|\nabla_h p^n\right\|_{L^2}^2\right)\right) \\
&\geq \frac{1}{8}\int_{\Omega}\phi^4 d\mathbf{x} + \frac{\epsilon^2}{2}\int_{\Omega}|\nabla_h\phi^{n+1}|^2 d\mathbf{x} - C(\epsilon,\Omega)\left(\left\|\phi^n\right\|_{H^1}^2 + 1\right) + C(\Delta t)\|\nabla_h\mu^{n+\frac{1}{2}}\|_{L^2}^2 \\
&\quad + C(\epsilon,\sigma,\Delta t)\left(\left\|\frac{\mathbf{v}^*+\mathbf{v}^n}{2}\right\|_{L^2}^2 + \left\|\nabla_h\left(\frac{\mathbf{v}^*+\mathbf{v}^n}{2}\right)\right\|_{L^2}^2 - \left(\left\|\mathbf{v}^n\right\|_{L^2}^2 + \left\|\nabla_h p^n\right\|_{L^2}^2\right)\right)
\end{aligned}
$$

by choosing $\nu = \phi^{n+1} - \phi^n$ in Eq. (35) and $\mathbf{u} = (\mathbf{v}^* + \mathbf{v}^n)/2$ in Eq. (36). Thus the mobility function is bounded. Let us consider the test function $\nu = 1$ in Eq. (35) and derive the following bounded inequality:

$$
\begin{aligned}
&\left|\int_{\Omega}\mu^{n+\frac{1}{2}} d\mathbf{x}\right| = \left|\int_{\Omega} g(\phi^{n+1}) d\mathbf{x}\right| \\
&= \int_{\Omega}\frac{1}{4}\left|\phi^{n+1}\right|^4 - \frac{1}{2}\left|\phi^{n+1}\right|^3 + \frac{1}{4}\left|\phi^{n+1}\right|^2 - \frac{1}{4}\left|\phi^n\right|^4 - \frac{1}{2}\left|\phi^n\right|^3 - \frac{1}{4}\left|\phi^n\right|^2 d\mathbf{x} \\
&\leq \int_{\Omega}\frac{1}{4}|\phi^{n+1}|^3 + \frac{1}{4}|\phi^{n+1}|^2 d\mathbf{x} + C\left(\left\|\phi^n\right\|_{L^4}^4 + \left\|\phi^n\right\|_{L^3}^3 + \left\|\phi^n\right\|_{L^2}^2\right) \\
&\leq C\left(\|\phi^{n+1}\|_{L^3}^3 + \|\phi^{n+1}\|_{L^2}^2\right) + C\left(\left\|\phi^n\right\|_{L^4}^4 + \left\|\phi^n\right\|_{L^3}^3 + \left\|\phi^n\right\|_{L^2}^2\right) \\
&\leq C\left(\|\phi^{n+1}\|_{L^4}^3 + \|\phi^{n+1}\|_{L^4}^2\right) + C\left(\left\|\phi^n\right\|_{H^1}^4 + \left\|\phi^n\right\|_{H^1}^3 + \left\|\phi^n\right\|_{H^1}^2\right) \\
&\leq C\|\phi^{n+1}\|_{L^4}^3 + C\left(\left\|\phi^n\right\|_{H^1}^4 + \left\|\phi^n\right\|_{H^1}^3 + \left\|\phi^n\right\|_{H^1}^2 + 1\right)
\end{aligned}
\tag{41}
$$

by yielding the Young's inequality. Thus we can obtain the estimation $|m(\mu^{n+\frac{1}{2}})|^{4/3} \leq C\|\phi^{n+1}\|_{L^4}^4 + C$ by performing the Hölder's inequality, where $m(\mu^{n+\frac{1}{2}}) := \int_{\Omega}\mu^{n+\frac{1}{2}} d\mathbf{x}/|\Omega|$ in $H^1(\Omega)$. By applying the Poincaré inequality, we can derive $\langle \mathcal{G}(\mu^{n+\frac{1}{2}}), \mu^{n+\frac{1}{2}}\rangle \geq C\|\mu^{n+\frac{1}{2}}\|_{H^1}^{4/3} - C$, which corresponds to the coercivity of $\mathcal{G}$ as

$$
\lim_{\|\mu^{n+\frac{1}{2}}\|_{H^1}\to\infty} \frac{\langle \mathcal{G}(\mu^{n+\frac{1}{2}}), \mu^{n+\frac{1}{2}}\rangle}{\|\mu^{n+\frac{1}{2}}\|_{H^1}} \to \infty. \tag{42}
$$

Herein, we have derive the boundedness, the monotonicity, and the coercivity of the operator $\mathcal{G}$. By taking the Browder–Minty Lemma 1, we can yield that there exists a unique solution $\mu \in H^1(\Omega)$ such that $\langle \mathcal{G}(\mu), \nu\rangle = 0, \forall \nu \in H^1(\Omega)$ and the corresponding $\phi \in H^1(\Omega), \mathbf{v}^* \in \mathbf{H}_0^1$ uniquely solve the system Eq. (34), (35), and (36). This completes the proof. □

Remark 4. We should note that this paper does not provide the theoretical proof for the optimal rate convergence analysis and error estimate with the proposed numerical scheme due to limitations of space. The hybrid system Eq. (1) is coupled by the CH equation, incompressible NS equation, and the heat transfer equation, which can be solved by the decoupled discrete system Eq. (17). We suggest to refer to [52,53] for the investigation of convergence and error of discrete CHNS system, which are standard and the proofs are omitted. Furthermore, since the system considered in this paper is with the 'one-way' coupling manner, i.e., the temperature field is influenced by the relative velocity and phase field function while the surface tension and various physical parameters of the binary fluids are independent of temperature, the convergence analysis and error estimate of CHNS system in [52] can be directly generalized to our system. In the future work, we will consider the hybrid system with variable densities by a quasi-incompressible fluids flow and provide the rigorous theoretical proof of the convergence analysis and error estimates on arbitrary surfaces.

4. Numerical experiments

We perform various computational experiments to verify the efficiency and robustness of our proposed method. Unless otherwise specified, we will choose the following parameters for the numerical simulations: $\rho = 1$, $\eta = 1$, $C_p = 1$, $k = 1$,

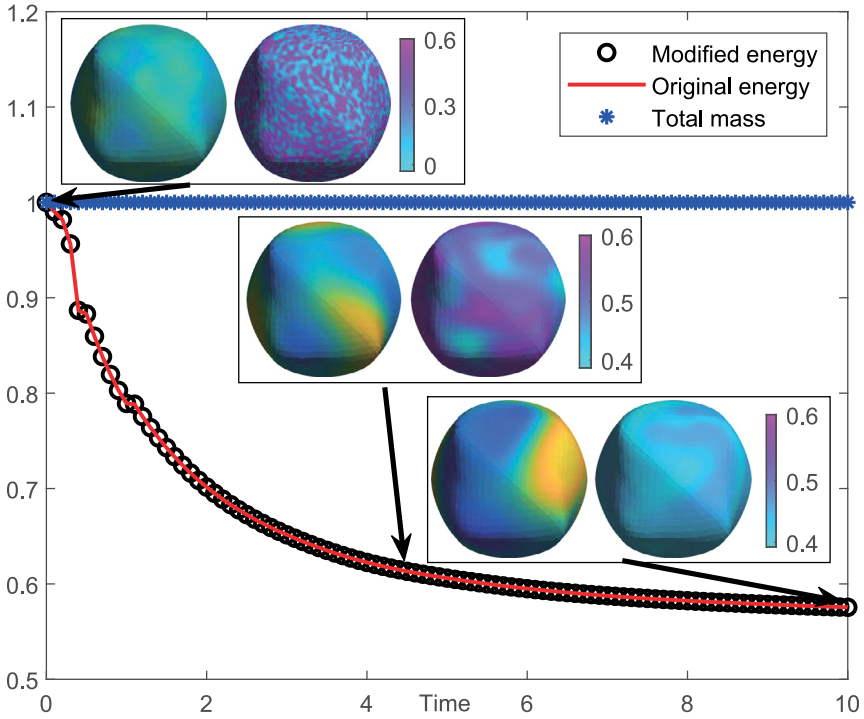

Fig. 2. Time evolution of the discrete modified and original energy, and mass conservation of the proposed method. The inset figures are the phase and temperature fields at the indicated times 0, 5 and 10, respectively. The modified energy and original energy have been normalized by the initial energy. The total mass has been normalized by the initial mass.

$Cn = 50$, $Re = 100$, $\epsilon = 5h/(4\sqrt{2}\text{atanh}(0.9))$, $Pe = 1/\epsilon$ and $\Delta t = 0.1h$. Since we consider closed surfaces, there is no boundary conditions for this system.

4.1. Unconditional energy dissipation

In this subsection, we demonstrate the mass conservation and unconditional energy dissipation in Fig. 2 to imply that the proposed scheme is indeed unconditionally stable. We consider the numerical test on a deformed cube over the domain $(0, 1) \times (0, 1)$. The initial conditions are given as

$$\begin{cases} \phi(x, y, z, 0) = \text{rand}(x, y, z), \quad T(x, y, z, 0) = \phi(x, y, z, 0), \quad p(x, y, z, 0) = 0, \\ u(x, y, z, 0) = 0, \quad v(x, y, z, 0) = 0, \quad w(x, y, z, 0) = 0, \end{cases} \tag{43}$$

where rand (x, y, z) is a random number between 0 and 1. The computation is run up to $t = 10$ with time step $\Delta t = 0.01$. The modified energy and original energy have been normalized by the initial energy. The total mass has been normalized by the initial mass. As can be seen from Fig. 2, the modified energy curve and the original energy curve decay with respect to time. The mass conservation of the entire system is satisfied during the evolution. The inset sub-figures are the morphology of the phase-field and the temperature field at the indicated times 0, 5 and 10, respectively. From the sub-figures, we can obviously see that the phase separation converges rapidly and the temperature field becomes uniform under the influence of the phase-field. Furthermore, to demonstrate the divergence free condition is satisfied during the computation, we applied the calculation of the average divergence of the total points over the deformed cube. The divergence-free condition is significant for the incompressible NS equation of the proposed system. The projection method coupled with Helmholtz–Hodge decomposition applied in this paper has been proved theoretically to satisfy the divergence-free condition. We should note that direct methods are limited by the quality of the surface mesh. A high quality mesh should be used to obtain a good solution. In addition, the higher the mesh quality is, the faster the convergence rate will be. Based on current computer aided design technologies, the mesh quality can basically meet our requirements. Our method has few requirements on the mesh quality and works well with the poor mesh, which can refer to our previous work [30,32]. The average divergence at the indicated times $t = 1$, 5 and 10 are $2.71\text{e}-4$, $1.76\text{e}-4$ and $7.74\text{e}-5$, respectively, which confirms that our system is indeed divergence free.

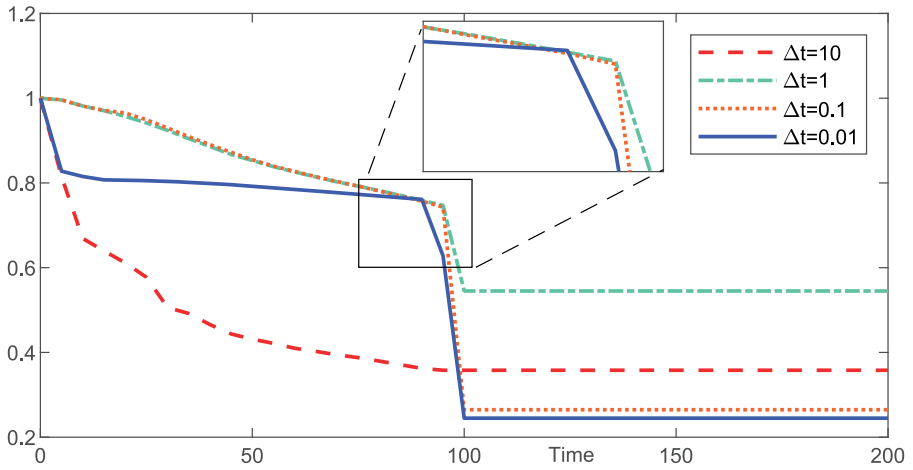

Fig. 3. Time evolution of the normalized free energy functional of the proposed model for $\Delta t = 10$, 1, 0.1 and 0.01.

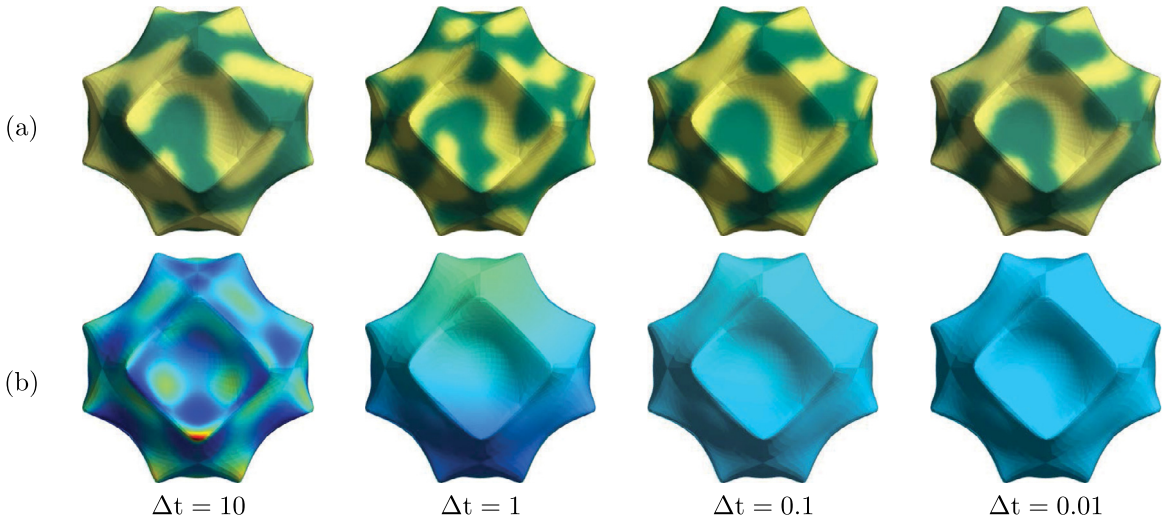

Fig. 4. The results of (a) the phase field and (b) the temperature field with different time steps. From left to right, the chosen time step is $\Delta t = 10$, 1, 0.1 and 0.01, respectively.

4.2. Numerical stability performance of the proposed scheme

In this subsection, we perform a comparison test to inspect the stability of the proposed system with different time steps. The numerical test is applied on the complicated stellated manifold over the domain $(0, 1) \times (0, 1)$. The initial conditions are chosen as

$$\begin{cases} \phi(x, y, z, 0) = \text{rand}(x, y, z), \quad T(x, y, z, 0) = 0.5 + 0.5 \sin(2\pi x) \sin(2\pi y) \sin(2\pi z), \\ u(x, y, z, 0) = 0, \quad v(x, y, z, 0) = 0, \quad w(x, y, z, 0) = 0, \end{cases} \tag{44}$$

where rand (x, y, z) is a random number between 0 and 1. The computation is run up to $t = 200$ for different time steps $\Delta t = 10$, 1, 0.1 and 0.01, respectively. We plot the four curves of the original energy in Fig. 3 until the indicated time $t = 200$. No blow-up of the numerical solutions have been shown and the discrete original energies with different time steps are non-increasing with respect to time, which implies that we can use large time step for the numerical simulations. Furthermore, the results obtained by using $\Delta t = 0.1$ have shown the same trend with the results of smaller time step $\Delta t = 0.01$, while these differ from the results with the larger time step $\Delta t = 1$. These results imply that large time step will leads to less accurate results because large error of the numerical solutions have been obtained compared with those with small time step. Thus, we suggest to use a small time step for high accurate numerical solutions. In this paper, we use an appropriate value for Δt is $\Delta t = 0.1$ to obtain the accuracy of the proposed scheme and reduce computational costs (see Fig. 4).

Table 1
Errors and convergence rates with different time steps for velocity field u and v of Stokes equation, phase field ϕ of the CH equation and temperature field T of HT equation.

Δt	Error					Order				
	u	v	w	ϕ	T	u	v	w	ϕ	T
8e − 04	8.73e − 05	6.42e − 05	3.42e − 04	1.47e − 06	1.72e − 05	–	–	–	–	–
4e − 04	2.13e − 05	1.53e − 05	7.95e − 05	3.42e − 07	4.65e − 06	2.0	2.1	2.1	2.1	1.9
2e − 04	5.46e − 06	4.03e − 06	1.89e − 05	9.50e − 08	1.03e − 06	2.0	1.9	2.1	1.8	2.2
1e − 04	1.44e − 06	9.83e − 07	5.11e − 06	2.29e − 08	2.64e − 07	1.9	2.0	1.9	2.1	2.0

Table 2
Errors and convergence rates with different space steps for velocity field u and v of Stokes equation, phase field ϕ of CH equation and temperature field T of HT equation.

h	Error					Order				
	u	v	w	ϕ	T	u	v	w	ϕ	T
2.0e − 01	2.45e − 03	3.41e − 03	6.82e − 02	7.15e − 04	7.24e − 03	–	–	–	–	–
1.0e − 01	5.44e − 04	6.93e − 04	1.41e − 02	2.24e − 04	1.41e − 03	2.2	2.3	2.3	1.7	2.4
5.0e − 02	1.12e − 04	2.02e − 04	3.89e − 03	4.97e − 05	4.14e − 04	2.3	1.8	1.9	2.2	1.8
2.5e − 02	3.32e − 05	4.65e − 05	8.96e − 04	1.28e − 05	1.08e − 04	1.8	2.1	2.1	2.0	1.9

4.3. Convergence test

In this subsection, two numerical experiments have been applied to verify the convergence of our proposed numerical scheme, which have second-order accuracy in time and space. To avoid the derivative influence of the topology structure of the involved manifold, a unit sphere has been used to generate a series of high-quality mesh-grids, which satisfy the properties of Delaunay triangles. To test the temporal accuracy of the proposed method, we take a set of different temporal steps Δt =8e − 4, 4e − 4, 2e − 4 and 1e − 4 with the same spatial steps h = 2.5e − 2. We run the program until time $t = 0.1$ with the same initial condition:

$$\begin{cases} \phi(x,y,z,0) = 0.5 + 0.5\sin(2\pi x)\sin(2\pi y)\sin(2\pi z),\ T(x,y,z,0) = \cos(2\pi x)\cos(2\pi y)\cos(2\pi z), \\ u(x,y,z,0) = \cos(2\pi x)\sin(2\pi y)\sin(2\pi z),\ v(x,y,z,0) = \sin(2\pi x)\cos(2\pi y)\sin(2\pi z), \\ w(x,y,z,0) = \sin(2\pi x)\sin(2\pi y)\cos(2\pi z),\ p(x,y,z,0) = 0. \end{cases}$$

The parameters are chosen as $\epsilon = 0.03$, $\sigma = \epsilon/10$, $\rho = 1$, $\eta = 1$. Since there are no closed-form analytical solution of the computational system, we assume that the result with a fine temporal step $\Delta t = 2e - 5$ as the reference solution $\phi^{\mathbf{ref}}$. Here, the error is defined as $e_{i,\Delta t} := \phi_{i,\Delta t} - \phi_i^{\mathbf{ref}}$. The rate of convergence is defined as the ratio of successive errors: $log_2(\|e_{i,\Delta t}\|_2/\|e_{i,\Delta t/2}\|_2)$. The errors and the rates of convergence are presented in Table 1. The results demonstrate the second-order temporal accuracy of the discrete scheme Eqs. (17). For the presentation of the second-order spatial accuracy of the discrete system, let us define $e_{i,h} := \phi_{i,d} - \left(\zeta_i\phi_p^{\mathrm{ref}} + \eta_i\phi_q^{\mathrm{ref}} + \theta_i\phi_r^{\mathrm{ref}}\right)$, where p, q and r are the fine reference grid indexes in the triangle and the weighting coefficients ζ, η, θ are determined by $\mathbf{v}_{i,d} := \zeta_i\mathbf{v}_p^{\mathrm{ref}} + \eta_i\mathbf{v}_q^{\mathrm{ref}} + \theta_i\mathbf{v}_r^{\mathrm{ref}}$. The results are listed in Table 2. Here, $\log_2\left(\left\|e_{i,h}\right\|_2 / \left\|e_{i,h/2}\right\|_2\right)$ is the convergence rate and Δt = 5e−4 is used. The results are computed until $t = 0.1$ and a reference solution is computed with a very fine space grid $h = 0.005$. The results listed in Table 2 imply that the proposed method is spatially second-order accurate.

4.4. Binary fluids flow on complex surfaces

In this subsection, we apply a numerical test for the surface computation over the complex surfaces. We choose the three complex mesh, i.e., a dupini-cyclide surface, a merged triply periodic minimal surface proposed in [54] and a porous cylinder surface, which consist of nonuniform and poor-quality mesh. Without loss of generality, the quality of the mesh grid will affect the accuracy of the solutions. The adaptive mesh may lead to the non-convergent solutions of the discrete operators, i.e., the discrete divergence operator, the gradient operator and the Laplace–Beltrami operator, over the triangular surfaces. To show the significant robustness and efficiency of the proposed scheme for the surface computation, we implied the binary thermal fluids over the three surfaces as shown in Fig. 5. Here, the initial conditions are chosen as

$$\begin{cases} \phi(x,y,z,0) = \mathrm{rand}(x,y,z), \quad T(x,y,z,0) = \phi(x,y,z,0), \\ u(x,y,z,0) = 0,\ \ v(x,y,z,0) = 0,\ \ w(x,y,z,0) = 0,\ \ p(x,y,z,0) = 0. \end{cases} \tag{45}$$

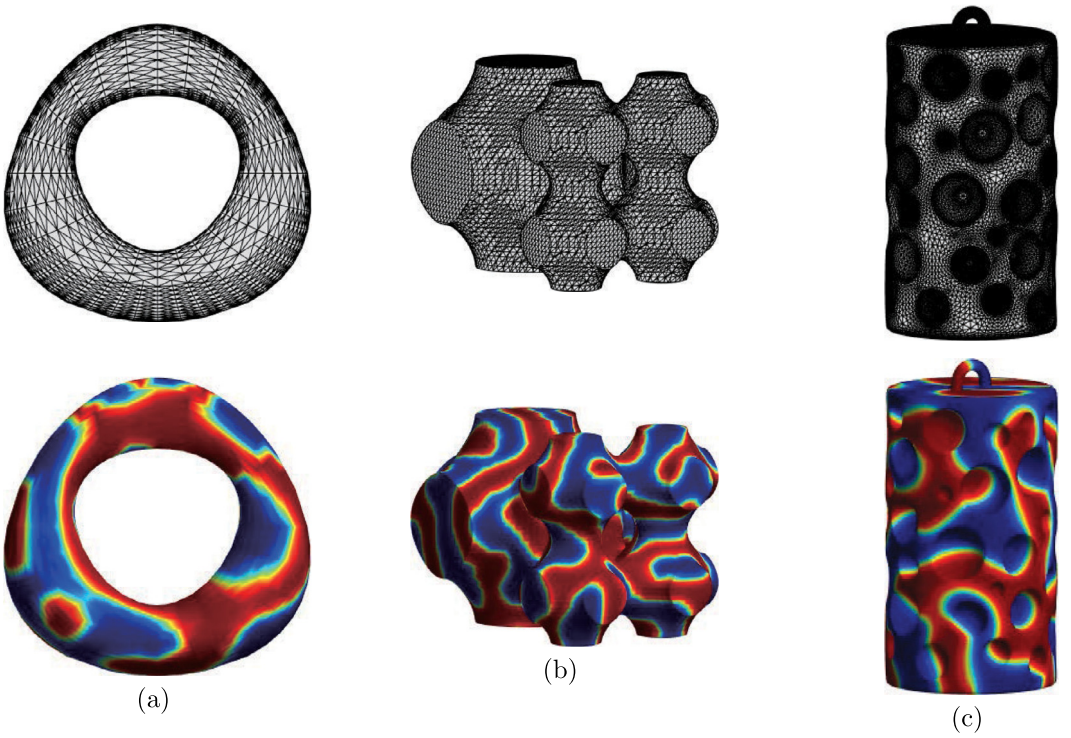

Fig. 5. Spinodal decomposition over three complex mesh, i.e., (a) a dupini-cyclide surface, (b) a merged triply periodic minimal surface and (c) a porous cylinder surface, which consist of nonuniform and poor-quality mesh. The top row is the surface mesh structure and the bottom row is the final plots of phase-field until time $t = 20$.

The parameters are chosen as follows: $\Delta t = 0.1$, $\epsilon = 0.005$, $Pe = 1/\epsilon$, $\sigma = 10$, $\rho = 1$ and $\eta = 1$. As shown in the top row of Fig. 5, the meshes of the three complex surfaces are with nonuniform mesh, which is of poor quality in somewhere. The bottom row shows the final plots of phase-field until time $t = 20$. It is obvious that the proposed method can work well for the surface computation over arbitrary meshes with nonuniform and poor-quality mesh grid.

4.5. Deformation of a complex droplet under shear flow and the heat transfer

In this subsection, we applied a deformation test to demonstrate the shape relaxation and the dynamic behaviors under shear background flow based on the proposed method. For this numerical experiment, we set the initial conditions as

$$\begin{cases} \phi(x,y,z,0) = 0.5 + 0.25\tanh((|x-0.5| + |y| - |z| + 0.5)/(\sqrt{5}\epsilon)) \\ \qquad\qquad + 0.25\tanh((|z-0.8| + |y| - |z| + 0.5)/(\sqrt{5}\epsilon)), \\ u(x,y,z,0) = 3yz,\ \ v(x,y,z,0) = -3xz,\ \ w(x,y,z,0) = 0,\ \ p(x,y,z,0) = 0, \\ T(x,y,z,0) = \phi(x,y,z,0). \end{cases} \tag{46}$$

The parameters are chosen as: $h = 0.04$, $\mathrm{dt} = 0.1h$, $Re = 1$, $Pe = 1/\epsilon$, $\sigma = 0.0001$, $\rho = 1$, $\eta = 1$, $c_P = 250$ and $k = 10$. As can be seen from Eq. (46), the velocities of the upper and lower parts of the manifold are opposite. We demonstrate the results of droplet under shear flow background velocity in Fig. 6. From left to right, the indicated times are $t = 0$, 1, 4 and 20, respectively. Fig. 6(a) shows the evolutions of the phase-field. As we can see, the isolated irregular interface becomes to a circle because of the isotropy of the mobility and the influence of surface tension. Then the interface of the droplet becomes twisted until the fracture appears because of the small surface tension and high velocity at the tip of drop. Fig. 6(b) shows the evolutions of the temperature field. It is obvious that the temperature field rotates under the shear flow to transfer heat, and eventually diffuses across the whole surface. The results shown in Fig. 6. correspond with the physical context, which implies that the proposed method is indeed effective. Furthermore, we compare the temperature of the background velocity with or without shear flow in Fig. 7 from the vertical view at the indicated times $t = 0$, 1, 4 and 20, respectively. The initial conditions are the same with Fig. 6. From Fig. 7(a) we can clearly observe that the thermal flow rotates around the sphere and eventually stabilizes under the influence of shear flow. Comparing with Fig. 7(a), the results without shear flow background velocity show that the thermal fluid diffused uniformly along the droplet boundary, which corresponds to the physical context.

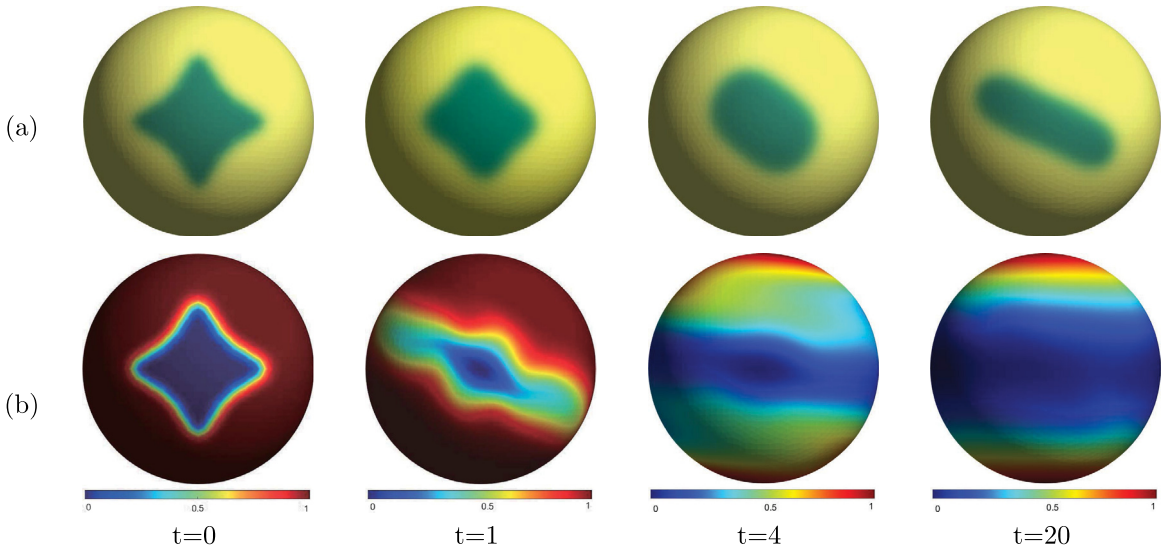

Fig. 6. The temporal evolution of (a) phase-field and (b) temperature field under shear flow. From left to right, the indicated times are $t = 0$, 1, 4 and 20, respectively.

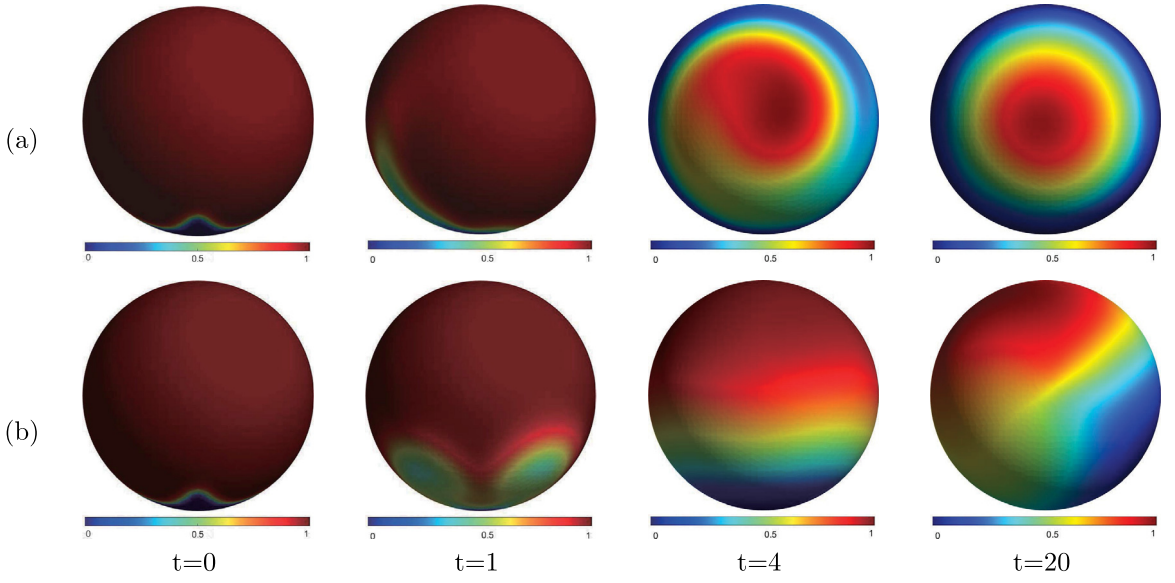

Fig. 7. The comparison of the dynamic behaviors of the temperature field with or without shear flow. (a) is the evolution with shear flow and (b) is the evolution without shear flow, respectively. From left to right, the indicated times are $t = 0$, 1, 4 and 20, respectively.

4.6. Spinodal decomposition in an arbitrary domain over surfaces

In this subsection, we applied a numerical test for the inspection of the proposed method in an arbitrary domain of the computational surface. As can be seen in Fig. 8, we fixed two circular domains on a sphere, which does not belong to the computational domain. For testing the efficiency of the proposed method, we set the initial conditions as following:

$$\begin{cases} \phi(x, y, z, 0) = \text{rand}(x, y, z), \quad T(x, y, z, 0) = \phi(x, y, z, 0), \\ u(x, y, z, 0) = 0, \quad v(x, y, z, 0) = 0, \quad w(x, y, z, 0) = 0. \end{cases} \tag{47}$$

The results are run up to time $t = 10$ and we demonstrate the results of the indicated times $t = 0$, 1, 5 and 10, respectively. It is obvious to see that the binary fluids on the surface first converge under the influence of surface tension($t = 1$). Then the binary fluids around the fixed domain under the action of the velocity field($t = 5$). The stable state has been obtained

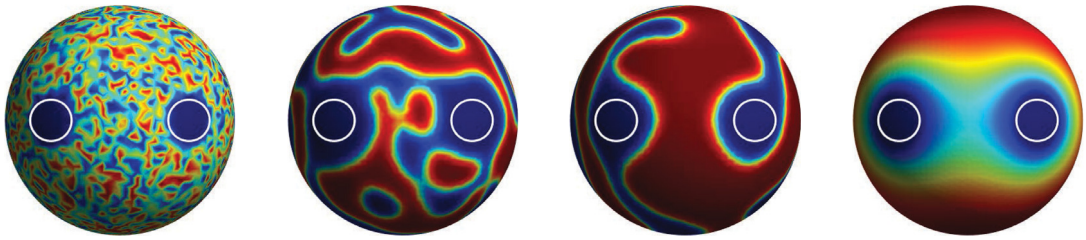

Fig. 8. The spinodal decomposition in an arbitrary domain over the sphere mesh grid. From left to right, the indicated times are $t = 0$, 1, 5 and 10, respectively.

after $t = 10$ with complete separation of the binary fluids system. This experiment shows that our method can be used to work in arbitrary domain over arbitrary surfaces.

4.7. Simulation of different buoyancy-driven flow on surfaces

To show the performance of the proposed scheme in simulating a binary fluids under different buoyancy-driven flow, we applied two long-time evolutions to simulate the motions of the droplet over surfaces. There are two forms of generalized buoyancy-flow in the system of this paper, one is the Boussinesq flow with thermal convection and the other is the gravity-driven flow with big density ratio.

4.7.1. Boussinesq flow with thermal convection

In this subsection, we perform a thermodynamic system test based on the Boussinesq dynamic equation. This system reflects that the thermal convection affects the fluid motion through the gravity term [55], which has the following form:

$$\begin{aligned}&\rho_i^{n+\frac{1}{2}}\left(\frac{\mathbf{v}_i^*-\mathbf{v}_i^n}{\Delta t}+\frac{1}{2}\widetilde{\mathbf{v}}_i^{n+\frac{1}{2}}\cdot\nabla_h(\frac{1}{2}\mathbf{v}_i^*+\frac{1}{2}\mathbf{v}_i^n)+\frac{1}{2}\nabla_h\cdot\left(\widetilde{\mathbf{v}}_i^{n+\frac{1}{2}}\otimes(\frac{1}{2}\mathbf{v}_i^*+\frac{1}{2}\mathbf{v}_i^n)\right)\right)\\&=\nabla_h\cdot\left(\eta_i^{n+\frac{1}{2}}\left(\nabla_h(\frac{1}{2}\mathbf{v}_i^*+\frac{1}{2}\mathbf{v}_i^n)\right)\right)-\nabla_h p_i^n-\frac{\sigma}{\epsilon}\widetilde{\phi}_i^{n+\frac{1}{2}}\nabla_h\mu_i^{n+\frac{1}{2}}+\alpha(T_i^{n+\frac{1}{2}})\mathbf{g}.\end{aligned}$$

Here, we denote $\mathbf{g} \coloneqq (0,\ 0,\ -1)$ as the gravity acceleration and α is the coefficient of the heating effect. To imply the robustness of the proposed method, we choose the initial conditions as:

$$\begin{cases}\phi = 0.5 - 0.5\tanh((|x-1|+|y|+|z|-0.8)/(\sqrt{5}\epsilon)), \quad T(x,y,z,0)=\phi(x,y,z,0),\\ u(x,y,z,0)=0, \quad v(x,y,z,0)=0, \quad w(x,y,z,0)=0,\end{cases}$$

The non-default parameters are chosen as: $h = 0.04$, $\Delta t = 0.01$, $\epsilon = 0.08$, $Pe = 1/\epsilon$ and $\sigma = 1000$, ρ and η are constant. We have demonstrated the results of phase-field and the temperature field in Fig. 9. The procedure runs up to time $t = 5$ and the indicated times are chosen as $t = 0$, 1.5, 2.5 and 5, respectively. As can be seen from Fig. 9(a), since the temperature of the droplet is higher than that of the fluid equilibrium state, the heat convection causes the droplet to move upward. Meanwhile, the isolated irregular interface relaxes to a circle under the influence of the surface tension. For this numerical test, we ignore the influence of static pressure on the heat convection of the Boussinesq fluid, which causes the immigration of the static instability of the stratified fluid. The evolution of the temperature field has been shown in Fig. 9(b). It is obvious that the thermal flow produces Rayleigh–Taylor instability [56] with the droplet movement. This phenomena occurs at the interface between two fluids of different velocity when a small disturbance appears. These results show that the proposed mode can handle the convection problem caused by heat conduction well.

4.7.2. Gravity-driven flow with big density ratio

In this subsection, we simulate rising process under the gravity-driven flow over a star surface. We add a gravity force term to the NS equation as follows:

$$\begin{aligned}&\rho(\phi_i^{n+\frac{1}{2}})\frac{\mathbf{v}_i^*-\mathbf{v}_i^n}{\Delta t}+\frac{\rho(\phi_i^{n+\frac{1}{2}})}{2}\left(\widetilde{\mathbf{v}}_i^{n+\frac{1}{2}}\cdot\nabla_h(\frac{1}{2}\mathbf{v}_i^*+\frac{1}{2}\mathbf{v}_i^n)+\nabla_h\cdot\left(\widetilde{\mathbf{v}}_i^{n+\frac{1}{2}}\otimes(\frac{1}{2}\mathbf{v}_i^*+\frac{1}{2}\mathbf{v}_i^n)\right)\right)\\&=-\nabla_h p_i^n+\nabla_h\cdot\left(\eta\nabla_h(\frac{1}{2}\mathbf{v}_i^*+\frac{1}{2}\mathbf{v}_i^n)\right)-\frac{\sigma\rho(\phi_i^{n+\frac{1}{2}})}{\epsilon}\widetilde{\phi}_i^{n+\frac{1}{2}}\nabla_h\mu_i^{n+\frac{1}{2}}+\frac{\rho(\phi_i^{n+\frac{1}{2}})-\rho_1}{Fr^2}\mathbf{g},\end{aligned}$$

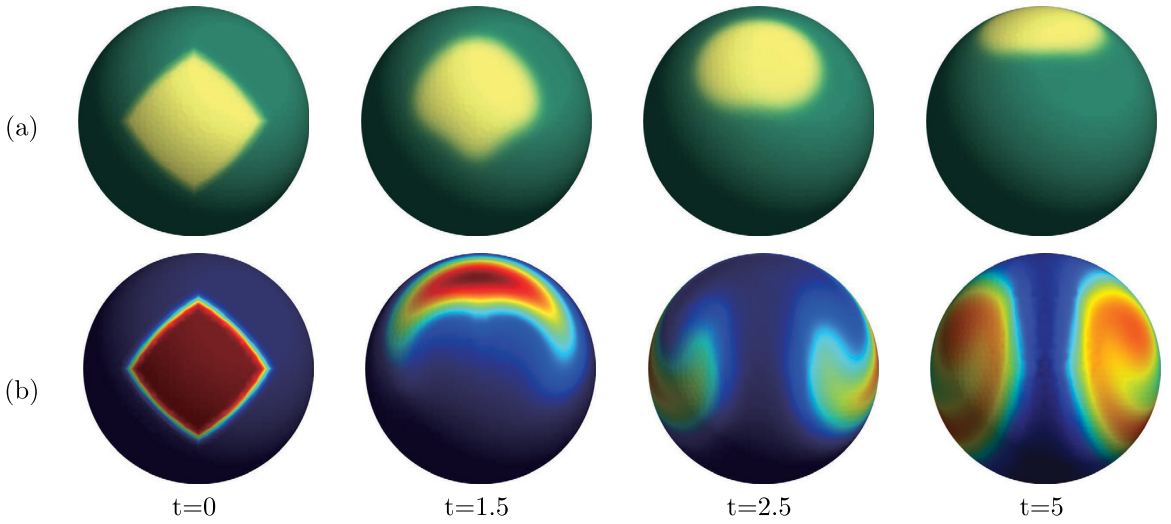

Fig. 9. Simulation of Boussinesq flow with thermal convection over a sphere surface. From the left to right, the indicated times are $t = 0$, 1.5, 2.5 and 5, respectively. (a) is the evolution of the phase-field. (b) is the evolution of the temperature field.

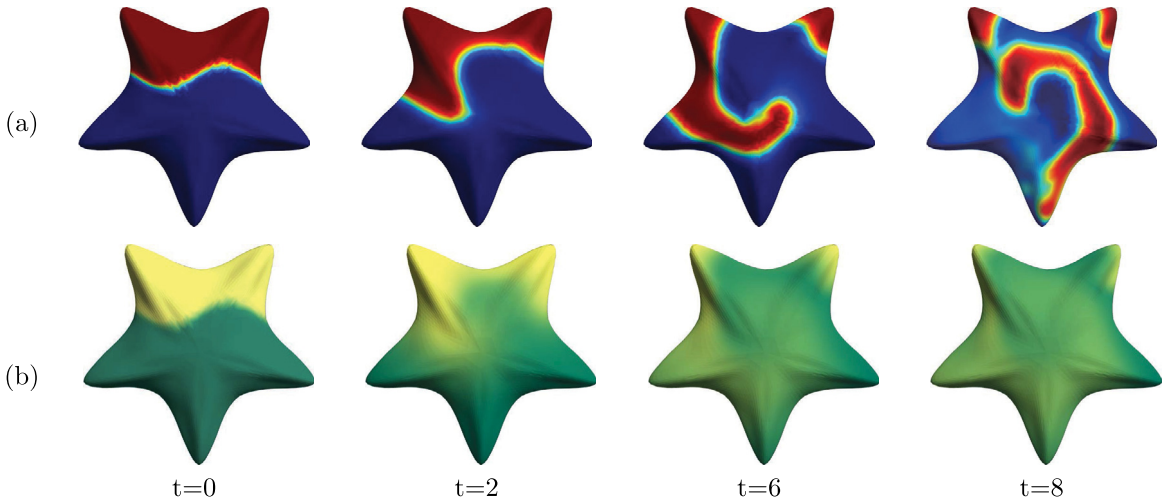

Fig. 10. Simulation of gravity-driven flow over a star surface. From the left to right, $t = 0$, 6 and 12, respectively. (a) is the evolution of the phase-field. (b) is the evolution of the temperature field.

where $\rho = \rho_1\phi + \rho_2(1-\phi)$, ρ_1 and ρ_2 are the densities of two phases and $\rho_1 \leq \rho_2$. We use $\mathbf{g} := (0,\ 0,\ -1)$ and Fr is the Froude number. It should be pointed out that the modified system still has second-order accuracy with respect to time and space based on the applied Crank–Nicolson method. The initial conditions are defined as

$$\begin{cases} \phi(x,y,z,0) = 0.5 + 0.5\tanh\left(\dfrac{z - 0.6 + 0.01\sin(4\pi x)}{\sqrt{2}\epsilon}\right), T(x,y,z,0) = \phi(x,y,z,0), \\ u(x,y,z,0) = v(x,y,z,0) = w(x,y,z,0) = 0,\ \ p(x,y,z,0) = 0. \end{cases}$$

Here, the following parameters are used: $h = 0.001$, $dt = h$, $\epsilon = 0.002$, $Pe = 1/\epsilon$, $Fr = 0.5$. For this test, we omit the surface tension. It is well known that the spike structure will be obtained when a heavier fluid is located above the lighter fluid and a small disturbance appears on the interface [35]. As can be seen from Fig. 10(a), the density of the red domain is bigger than that of the blue domain. Under the influence of gravity, the positions of binary fluid flows have changed along the star surface. As we expected, the phase of big density moves downward while the one of small density moves reversely. Meanwhile, the Rayleigh–Taylor instability and the Kelvin–Helmholtz instability has appeared during the evolution, which caused by the big density ratio and the velocity difference. As can be seen in Fig. 10(b), the temperature of the whole computational domain reaches equilibrium as the fluid flows. This simulation indicates that our method can be effectively used for the computation with gravity-driven flow.

5. Conclusion

In this paper, we have proposed a novel scheme for the surface computation of simulating thermal flow motion on arbitrary surfaces. The coupling system is combined by the heat transfer equation with the incompressible NS equation based on the phase-field model. The complicated system is decouple by the proposed method and converted to be a linear system, which can be solved by a biconjugate gradient stabilized method. We constructed the corresponding discrete operators, i.e., discrete gradient operator, discrete divergence operator and Laplace–Beltrami operator, over the arbitrary surfaces, which have the provable second-order accuracy for the spatial discretization. For the seconder-order temporal accuracy, we discretize the solution equations by the Crack–Nicolson-type method. The Picard iteration method is applied for the pressure Poisson type equation to confirm the accuracy of the solution. The discrete system is proved to be unconditionally stable, which means the algorithm is not restricted by the time step. The proposed framework provides a heuristic guidance for solving multiple physical field coupling problems on arbitrary manifold. Various numerical experiments have been demonstrated to verified the energy stability of this system and the second-order accuracy of the discrete scheme. In the future work, we will couple the temperature field with the phase field and velocity field to consider the thermal convection and provide the detailed optimal rate convergence analysis and error estimate theoretically.

CRediT authorship contribution statement

Qing Xia: Conceptualization, Methodology, Software, Investigation, Visualization, Writing – original draft. **Yuehan Liu:** Conceptualization, Methodology, Writing – original draft. **Junseok Kim:** Conceptualization, Writing – review & editing, Supervision. **Yibao Li:** Conceptualization, Methodology, Software, Writing – review & editing, Supervision, Project administration.

Data availability

No data was used for the research described in the article.

Acknowledgments

The corresponding author (Y.B. Li) is supported by National Natural Science Foundation of China (No. 12271430). Q. Xia is supported by the Fundamental Research Funds for the Central Universities, China (No. XYZ022022005). J.S. Kim was supported by Basic Science Research Program through the National Research Foundation of Korea (NRF) funded by the Ministry of Education (NRF-2019R1A2C1003053). The authors would like to thank the reviewers for their constructive and helpful comments regarding the revision of this article.

Appendix

In this section, we provide the proof of $\Delta_h X(\mathbf{G}_j) = 0$ in Eq. (9). Let us begin with the Cramer's rule, we can be obtain the follows:

$$\Delta_h X\left(\mathbf{G}_j\right) = \frac{2}{|\mathbf{B}_i|} A. \tag{48}$$

Here

$$\begin{aligned} A = & \left(p_{j,j}p_{j+1,j+1} - p_{j+1,j}p_{j,j+1}\right)\left(\mathbf{X}(\mathbf{p}) - \mathbf{X}\left(\mathbf{G}_j\right)\right) \\ & - \left(p_{j,0}p_{j+1,j+1} - p_{j+1,0}p_{j,j+1}\right)\left(\mathbf{X}\left(\mathbf{p}_j\right) - \mathbf{X}\left(\mathbf{G}_j\right)\right) \\ & + \left(p_{j,0}p_{j+1,j} - p_{j+1,0}p_{j,j}\right)\left(\mathbf{X}\left(\mathbf{p}_{j+1}\right) - \mathbf{X}\left(\mathbf{G}_j\right)\right), \end{aligned} \tag{49}$$

where the following notations are denoted:

$$\begin{aligned} & p_{j,0} = \left\langle \mathbf{p}_j - \mathbf{G}_j, \mathbf{p} - \mathbf{G}_j \right\rangle, \ p_{j,j} = \left\langle \mathbf{p}_j - \mathbf{G}_j, \mathbf{p}_j - \mathbf{G}_j \right\rangle, \ p_{j,j+1} = \left\langle \mathbf{p}_j - \mathbf{G}_j, \mathbf{p}_{j+1} - \mathbf{G}_j \right\rangle, \\ & p_{j+1,0} = \left\langle \mathbf{p}_{j+1} - \mathbf{G}_j, \mathbf{p} - \mathbf{G}_j \right\rangle, \ p_{j+1,j} = \left\langle \mathbf{p}_{j+1} - \mathbf{G}_j, \mathbf{p}_j - \mathbf{G}_j \right\rangle, \ p_{j+1,j+1} = \left\langle \mathbf{p}_{j+1} - \mathbf{G}_j, \mathbf{p}_{j+1} - \mathbf{G}_j \right\rangle. \end{aligned} \tag{50}$$

Since G_j is the centroid of the triangle consisted by $\mathbf{p}$, $\mathbf{p}_j$, and $\mathbf{p}_{j+1}$, which yields that $\mathbf{X}(G_j) = (\mathbf{X}(\mathbf{p}) + \mathbf{X}(\mathbf{p}_j) + \mathbf{X}(\mathbf{p}_{j+1}))/3$. Thus we can rewrite Eq. (49) as follows:

$$\begin{aligned} A = & \left(-\left(p_{j,0}p_{j+1,j} - p_{j,j}p_{j+1,0}\right) - \left(p_{j,j+1}p_{j+1,0} - p_{j,0}p_{j+1,j+1}\right) + 2\left(p_{j,j}p_{j+1,j+1} - p_{j,j+1}p_{j+1,j}\right)\right)\frac{\mathbf{X}(\mathbf{p})}{3} \\ & \left(-\left(p_{j,0}p_{j+1,j} - p_{j,j}p_{j+1,0}\right) + 2\left(p_{j,j+1}p_{j+1,0} - p_{j,0}p_{j+1,j+1}\right) - \left(p_{j,j}p_{j+1,j+1} - p_{j,j+1}p_{j+1,j}\right)\right)\frac{\mathbf{X}(\mathbf{p}_j)}{3} \\ & \left(2\left(p_{j,0}p_{j+1,j} - p_{j,j}p_{j+1,0}\right) - \left(p_{j,j+1}p_{j+1,0} - p_{j,0}p_{j+1,j+1}\right) - \left(p_{j,j}p_{j+1,j+1} - p_{j,j+1}p_{j+1,j}\right)\right)\frac{\mathbf{X}(\mathbf{p}_{j+1})}{3} \\ = & Par_1\frac{\mathbf{X}(\mathbf{p})}{3} + Par_2\frac{\mathbf{X}(\mathbf{p}_j)}{3} + Par_3\frac{\mathbf{X}(\mathbf{p}_{j+1})}{3}. \end{aligned}$$

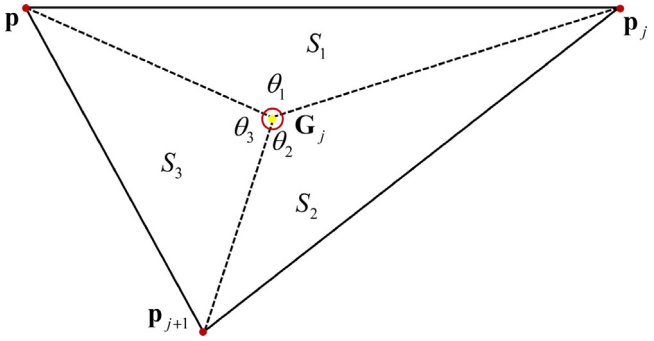

Fig. 11. Scheme diagram of arbitrary triangle consisted of $\mathbf{p}$, $\mathbf{p}_j$, and $\mathbf{p}_{j+1}$.

Let us define the following identities:

$$\begin{aligned} Par_1 &= -\Big(p_{j,0}p_{j+1,j} - p_{j,j}p_{j+1,0}\Big) - \Big(p_{j,j+1}p_{j+1,0} - p_{j,0}p_{j+1,j+1}\Big) + 2\Big(p_{j,j}p_{j+1,j+1} - p_{j,j+1}p_{j+1,j}\Big), \\ Par_2 &= -\Big(p_{j,0}p_{j+1,j} - p_{j,j}p_{j+1,0}\Big) + 2\Big(p_{j,j+1}p_{j+1,0} - p_{j,0}p_{j+1,j+1}\Big) - \Big(p_{j,j}p_{j+1,j+1} - p_{j,j+1}p_{j+1,j}\Big), \\ Par_3 &= 2\Big(p_{j,0}p_{j+1,j} - p_{j,j}p_{j+1,0}\Big) - \Big(p_{j,j+1}p_{j+1,0} - p_{j,0}p_{j+1,j+1}\Big) - \Big(p_{j,j}p_{j+1,j+1} - p_{j,j+1}p_{j+1,j}\Big). \end{aligned} \tag{51}$$

We first prove that $Par_1 = 0$, the other two equalities $Par_2 = 0$ and $Par_3 = 0$ can be straightforwardly obtained. We denote the angle between vector $\mathbf{p} - \mathbf{G}_j$ and vector $\mathbf{p}_j - \mathbf{G}_j$ as θ_1, denote the angle between vector $\mathbf{p}_j - \mathbf{G}_j$ and vector $\mathbf{p}_{j+1} - \mathbf{G}_j$ as θ_2, and denote the angle between vector $\mathbf{p}_{j+1} - \mathbf{G}_j$ and vector $\mathbf{p} - \mathbf{G}_j$ as θ_3, respectively. The schematic diagram has been shown in Fig. 11. We denote the area of triangle $\Delta_{\mathbf{G}_j\mathbf{p}\mathbf{p}_{j+1}}$, $\Delta_{\mathbf{G}_j\mathbf{p}_{j+1}\mathbf{p}_j}$, and $\Delta_{\mathbf{G}_j\mathbf{p}_j\mathbf{p}}$ as S_1, S_2, and S_3, respectively. Since $\mathbf{G}_j$ is the centroid of the triangle consisted of $\mathbf{p}$, $\mathbf{p}_j$, and $\mathbf{p}_{j+1}$, we can obtain

$$S_1 = S_2 = S_3, \tag{52}$$

which has been proved in [57].

Let us take the full expansion form for Par_1 as:

$$\begin{aligned} Par_1 &= -\Big(p_{j,0}p_{j+1,j} - p_{j,j}p_{j+1,0}\Big) - \Big(p_{j,j+1}p_{j+1,0} - p_{j,0}p_{j+1,j+1}\Big) + 2\Big(p_{j,j}p_{j+1,j+1} - p_{j,j+1}p_{j+1,j}\Big) \\ &= -\|\mathbf{p} - \mathbf{G}_j\|\|\mathbf{p}_j - \mathbf{G}_j\|^2\|\mathbf{p}_{j+1} - \mathbf{G}_j\|\cos\theta_1\cos\theta_2 + \|\mathbf{p} - \mathbf{G}_j\|\|\mathbf{p}_j - \mathbf{G}_j\|^2|\mathbf{p}_{j+1} - \mathbf{G}_j\|\cos\theta_3 \\ &\quad - \|\mathbf{p} - \mathbf{G}_j\|\|\mathbf{p}_j - \mathbf{G}_j\|\|\mathbf{p}_{j+1} - \mathbf{G}_j\|^2\cos\theta_2\cos\theta_3 + \|\mathbf{p} - \mathbf{G}_j\|\|\mathbf{p}_j - \mathbf{G}_j\|\|\mathbf{p}_{j+1} - \mathbf{G}_j\|^2\cos\theta_1 \\ &\quad + 2\Big(\|\mathbf{p}_j - \mathbf{G}_j\|^2\|\mathbf{p}_{j+1} - \mathbf{G}_j\|^2 - |\mathbf{p}_j - \mathbf{G}_j\|^2|\mathbf{p}_{j+1} - \mathbf{G}_j\|^2\cos^2\theta_2\Big) \\ &= \|\mathbf{p} - \mathbf{G}_j\|\|\mathbf{p}_j - \mathbf{G}_j\|\|\mathbf{p}_{j+1} - \mathbf{G}_j\|\Big(-\|\mathbf{p}_j - \mathbf{G}_j\|\cos\theta_1\cos\theta_2 + \|\mathbf{p}_j - \mathbf{G}_j\|\cos\theta_3 \\ &\quad - \|\mathbf{p}_{j+1} - \mathbf{G}_j\|\cos\theta_2\cos\theta_3 + \|\mathbf{p}_{j+1} - \mathbf{G}_j\|\cos\theta_1\Big) + 2\|\mathbf{p}_j - \mathbf{G}_j\|^2|\mathbf{p}_{j+1} - \mathbf{G}_j\|^2\sin^2\theta_2 \\ &= \|\mathbf{p} - \mathbf{G}_j\|\|\mathbf{p}_j - \mathbf{G}_j\|\|\mathbf{p}_{j+1} - \mathbf{G}_j\|\Big(-\|\mathbf{p}_j - \mathbf{G}_j\|\sin\theta_1\sin\theta_2 - \|\mathbf{p}_{j+1} - \mathbf{G}_j\|\sin\theta_2\sin\theta_3\Big) \\ &\quad + 2\|\mathbf{p}_j - \mathbf{G}_j\|^2\|\mathbf{p}_{j+1} - \mathbf{G}_j\|^2\sin^2\theta_2 \\ &= -\|\mathbf{p}_j - \mathbf{G}_j\|\|\mathbf{p}_{j+1} - \mathbf{G}_j\|\sin\theta_2\Big(\|\mathbf{p} - \mathbf{G}_j\|\|\mathbf{p}_j - \mathbf{G}_j\|\sin\theta_1 + \|\mathbf{p} - \mathbf{G}_j\|\|\mathbf{p}_{j+1} - \mathbf{G}_j\|\sin\theta_3\Big) \\ &\quad + 2\|\mathbf{p}_j - \mathbf{G}_j\|^2|\mathbf{p}_{j+1} - \mathbf{G}_j\|^2\sin^2\theta_2 \\ &= -2\|\mathbf{p}_j - \mathbf{G}_j\|^2|\mathbf{p}_{j+1} - \mathbf{G}_j\|^2\sin^2\theta_2 + 2\|\mathbf{p}_j - \mathbf{G}_j\|^2|\mathbf{p}_{j+1} - \mathbf{G}_j\|^2\sin^2\theta_2 = 0, \end{aligned}$$

where we have used the identity $\|\mathbf{p} - \mathbf{G}_j\|\|\mathbf{p}_j - \mathbf{G}_j\|\sin\theta_1 = \|\mathbf{p}_j - \mathbf{G}_j\|\|\mathbf{p}_{j+1} - \mathbf{G}_j\|\sin\theta_2 = \|\mathbf{p}_{j+1} - \mathbf{G}_j\|\|\mathbf{p} - \mathbf{G}_j\|\sin\theta_3$ due to Eq. (52). We can obtain that $Par_2 = 0$ and $Par_3 = 0$ in the same manner, which yields the following:

$$\Delta_h X\left(\mathbf{G}_j\right) = \frac{2}{|\mathbf{B}_i|}A = Par_1\frac{\mathbf{X}(\mathbf{p})}{3} + Par_2\frac{\mathbf{X}(\mathbf{p}_j)}{3} + Par_3\frac{\mathbf{X}(\mathbf{p}_{j+1})}{3} = 0. \tag{53}$$

This completes the proof.

References

[1] F. Mémoli, G. Sapiro, P. Thompson, Implicit brain imaging, NeuroImage 23 (2004) S179–S188.
[2] G.S. Ayton, J.L. McWhirter, P. McMurtry, G.A. Voth, Coupling field theory with continuum mechanics: a simulation of domain formation in giant unilamellar vesicles, Biophys. J. 88 (2005) 3855–3869.
[3] D. Halpern, O. Jensen, J. Grotberg, A theoretical study of surfactant and liquid delivery into the lung, J. Appl. Physiol. (1998).
[4] M. Hofer, H. Pottmann, Energy-minimizing splines in manifolds, in: ACM SIGGRAPH 2004 Papers, 2004, pp. 284–293.
[5] G. Zhao, S. Xu, W. Li, O.E. Teo, Fast variational design of multiresolution curves and surfaces with b-spline wavelets, Comput. Aided Des. 37 (2005) 73–82.
[6] S. Yoon, C. Lee, J. Park, D. Jeong, J. Kim, Uniformly distributed circular porous pattern generation on surface for 3d printing, Numer. Math.: Theory Methods Appl. 13 (2020) 845–862.
[7] F. Amiri, S. Ziaei-Rad, N. Valizadeh, T. Rabczuk, On the use of local maximum entropy approximants for Cahn–Hilliard phase-field models in 2d domains and on surfaces, Comput. Methods Appl. Mech. Engrg. 346 (2019) 1–24.
[8] G. Dziuk, Finite elements for the beltrami operator on arbitrary surfaces, in: Partial Differential Equations and Calculus of Variations, 1988, pp. 142–155.
[9] S. Yui, K. Hara, H. Zha, T. Hasegawa, A fast narrow band method and its application in topology-adaptive 3d modeling, in: International Conference on Pattern Recognition, Vol. 4, 2002, pp. 122–125.
[10] M. Cenanovic, P. Hansbo, M.G. Larson, Minimal surface computation using a finite element method on an embedded surface, Internat. J. Numer. Methods Engrg. 104 (2015) 502–512.
[11] S.G. Chen, J.Y. Wu, Discrete conservation laws on curved surfaces, SIAM J. Sci. Comput. 35 (2013) A719–A739.
[12] S.G. Chen, J.Y. Wu, Discrete conservation laws on evolving surfaces, SIAM J. Sci. Comput. 38 (2016) A1725–A1742.
[13] K. Marfurt, R. Kirlin, Narrow-band spectral analysis and thin-bed tuning, Geophysics 66 (2001) 1274–1283.
[14] M. Bertalmıo, L.T. Cheng, S. Osher, G. Sapiro, Variational problems and partial differential equations on implicit surfaces, J. Comput. Phys. 174 (2001) 759–780.
[15] J.B. Greer, An improvement of a recent eulerian method for solving PDES on general geometries, J. Sci. Comput. 29 (2006) 321–352.
[16] E.J. Fuselier, G.B. Wright, A high-order kernel method for diffusion and reaction–diffusion equations on surfaces, J. Sci. Comput. 56 (2013) 535–565.
[17] C.B. Macdonald, J. Brandman, S.J. Ruuth, Solving eigenvalue problems on curved surfaces using the closest point method, J. Comput. Phys. 230 (2011) 7944–7956.
[18] C.B. Macdonald, S.J. Ruuth, The implicit closest point method for the numerical solution of partial differential equations on surfaces, SIAM J. Sci. Comput. 31 (2010) 4330–4350.
[19] C. Piret, The orthogonal gradients method: A radial basis functions method for solving partial differential equations on arbitrary surfaces, J. Comput. Phys. 231 (2012) 4662–4675.
[20] Y. Li, C. Luo, B. Xia, J. Kim, An efficient linear second order unconditionally stable direct discretization method for the phase-field crystal equation on surfaces, Appl. Math. Model. 67 (2019) 477–490.
[21] S.G. Chen, J.Y. Wu, Discrete conservation laws on curved surfaces II: A dual approach, SIAM J. Sci. Comput. 36 (2014) A1813–A1830.
[22] X. Xiao, X. Feng, Z. Li, The local tangential lifting method for moving interface problems on surfaces with applications, J. Comput. Phys. 431 (2021) 110146.
[23] M. Sun, X. Feng, K. Wang, Numerical simulation of binary fluid-surfactant phase field model coupled with geometric curvature on the curved surface, Comput. Methods Appl. Mech. Engrg. 367 (2020) 113123.
[24] Y. Qin, C. Wang, C. Zhang, A positivity-preserving and convergent numerical scheme for the binary fluid-surfactant system, 2021, arXiv preprint arXiv:2102.08105.
[25] P. Suchde, J. Kuhnert, A fully lagrangian meshfree framework for PDEs on evolving surfaces, J. Comput. Phys. 395 (2019) 38–59.
[26] Q. Xia, G. Sun, Q. Yu, J. Kim, Y. Li, Thermal-fluid topology optimization with unconditional energy stability and second-order accuracy via phase-field model, Commun. Nonlinear Sci. Numer. Simul. 116 (2023) 106782.
[27] Q. Yu, Q. Xia, Y. Li, A phase field-based systematic multiscale topology optimization method for porous structures design, J. Comput. Phys. 466 (2022) 111383.
[28] Y. Li, Q. Xia, C. Lee, S. Kim, J. Kim, A robust and efficient fingerprint image restoration method based on a phase-field model, Pattern Recognit. 123 (2022) 108405.
[29] Y. Li, L. Zhang, Q. Xia, Q. Yu, J. Kim, An unconditionally energy-stable second-order time-accurate numerical scheme for the coupled Cahn–Hilliard system in copolymer/homopolymer mixtures, Comput. Mater. Sci. 200 (2021) 110809.
[30] Y. Li, J. Kim, N. Wang, An unconditionally energy-stable second-order time-accurate scheme for the Cahn–Hilliard equation on surfaces, Commun. Nonlinear Sci. Numer. Simul. 53 (2017) 213–227.
[31] Y. Li, R. Liu, Q. Xia, C. He, Z. Li, First-and second-order unconditionally stable direct discretization methods for multi-component Cahn–Hilliard system on surfaces, J. Comput. Appl. Math. 401 (2022) 113778.
[32] Q. Xia, Q. Yu, Y. Li, A second-order accurate, unconditionally energy stable numerical scheme for binary fluid flows on arbitrarily curved surfaces, Comput. Methods Appl. Mech. Engrg. 384 (2021) 113987.
[33] W. Chen, W. Feng, Y. Liu, C. Wang, S. Wise, A second order energy stable scheme for the Cahn–Hilliard–Hele–Shaw equations, 2016, arXiv preprint arXiv:1611.02967.
[34] Q. Xia, J. Kim, B. Xia, Y. Li, An unconditionally energy stable method for binary incompressible heat conductive fluids based on the phase field model, Comput. Math. Appl. 123 (2022) 26–39.
[35] J. Yang, J. Kim, A phase-field model and its efficient numerical method for two-phase flows on arbitrarily curved surfaces in 3d space, Comput. Methods Appl. Mech. Engrg. 372 (2020) 113382.
[36] R. Temam, Sur l'approximation de la solution des équations de Navier–Stokes par la méthode des pas fractionnaires (i), Arch. Ration. Mech. Anal. 32 (1969) 135–153.
[37] A. Alexandridis, L. Russo, D. Vakalis, G. Bafas, C. Siettos, Wildland fire spread modelling using cellular automata: evolution in large-scale spatially heterogeneous environments under fire suppression tactics, Int. J. Wildland Fire 20 (2011) 633–647.
[38] B. Bozzini, D. Lacitignola, I. Sgura, Spatio-temporal organization in alloy electrodeposition: a morphochemical mathematical model and its experimental validation, J. Solid State Electrochem. 17 (2013) 467–479.
[39] C. Samir, A. Srivastava, M. Daoudi, Automatic 3d face recognition using shapes of facial curves, in: IEEE Transactions on Pattern Analysis and Pattern Recognition, 2005.
[40] K. Morris, Design of finite-dimensional controllers for infinite-dimensional systems by approximation, 1994.
[41] G.A. Susto, M. Krstic, Control of PDE–ODE cascades with Neumann interconnections, J. Franklin Inst. B 347 (2010) 284–314.
[42] S. Tang, C. Xie, State and output feedback boundary control for a coupled PDE–ODE system, Systems Control Lett. 60 (2011) 540–545.
[43] E. Fridman, Y. Orlov, Exponential stability of linear distributed parameter systems with time-varying delays, Automatica 45 (2009) 194–201.

[44] J. Guermond, P. Minev, J. Shen, An overview of projection methods for incompressible flows, Comput. Methods Appl. Mech. Engrg. 195 (2006) 6011–6045.
[45] W. Chen, Y. Liu, C. Wang, S. Wise, Convergence analysis of a fully discrete finite difference scheme for the Cahn–Hilliard–Hele–Shaw equation, Math. Comp. 85 (2016) 2231–2257.
[46] Y. Liu, W. Chen, C. Wang, S. Wise, Error analysis of a mixed finite element method for a Cahn–Hilliard–Hele–Shaw system, Numer. Math. 135 (2017) 679–709.
[47] A. Kovtanyuk, A. Chebotarev, N. Botkin, K. Hoffmann, The unique solvability of a complex 3D heat transfer problem, J. Math. Anal. Appl. 409 (2014) 808–815.
[48] C. Liu, C. Wang, Y. Wang, A structure-preserving, operator splitting scheme for reaction–diffusion equations involving the law of mass action, J. Comput. Phys. 436 (2021) 110253.
[49] D. Han, X. Wang, A second order in time, uniquely solvable, unconditionally stable numerical scheme for Cahn–Hilliard–Navier–Stokes equation, J. Comput. Phys. 290 (2015) 139–156.
[50] E. Zeidler, Nonlinear functional analysis and its applications. II/B, in: Nonlinear Monotone Operators, Springer-Verlag, New York, 1990, Translated from the German by the author and Leo F. Boron.
[51] J. Shen, On error estimates of projection methods for Navier–Stokes equations: First-order schemes, SIAM J. Numer. Anal. 29 (1992) 57–77.
[52] A. Diegel, C. Wang, X. Wang, S. Wise, Convergence analysis and error estimates for a second order accurate finite element method for the Cahn–Hilliard–Navier–Stokes system, Numer. Math. 137 (2017) 495–534.
[53] W. Chen, S. Wang, Y. Zhang, D. Han, C. Wang, X. Wang, Error estimate of a decoupled numerical scheme for the Cahn–Hilliard–Stokes–Darcy system, IMA J. Numer. Anal. 42 (2022) 2621–2655.
[54] Y. Li, Q. Xia, S. Yoon, C. Lee, B. Lu, J. Kim, Simple and efficient volume merging method for triply periodic minimal structures, Comput. Phys. Comm. 264 (2021) 107956.
[55] X. Zheng, H. Babaee, S. Dong, C. Chryssostomidis, G. Karniadakis, A phase-field method for 3d simulation of two-phase heat transfer, Int. J. Heat Mass Transfer 82 (2015) 282–298.
[56] J. Kim, J. Lowengrub, Phase field modeling and simulation of three-phase flows, Interfaces Free Bound. 7 (2005) 435–466.
[57] P. Hammer, The centroid of a convex body, Proc. Amer. Math. Soc. 2 (1951) 522–525.